Greenland coastal air temperatures linked to Baffin Bay and Greenland Sea ice conditions during autumn through regional blocking patterns

Thomas J. Ballinger*

Department of Geography, Texas State University, San Marcos, TX, USA

Edward Hanna

School of Geography, University of Lincoln, UK

Richard J. Hall

Department of Geography, University of Sheffield, Sheffield, UK

Jeffrey Miller

Cryospheric Sciences Laboratory, NASA Goddard Space Flight Center, Greenbelt, MD, USA

Wyle, Inc, Houston, TX, USA

Mads H. Ribergaard and Jacob L. Høyer

Danish Meteorological Institute, Copenhagen, DK

Manuscript Submitted to *Climate Dynamics* on June 27, 2016

Revision Submitted December 20, 2016

Accepted February 11, 2017; doi: 10.1007/s00382-017-3583-3

*Corresponding Author's Address: 601 University Drive, San Marcos, Texas 78666, Phone: 512-245-3202, Email: tballinger@txstate.edu

Abstract

Variations in sea ice freeze onset and regional sea surface temperatures (SST) in Baffin Bay and Greenland Sea are linked to autumn surface air temperatures (SAT) around coastal Greenland through 500 hPa blocking patterns, 1979-2014. We find strong, statistically significant correlations between Baffin Bay freeze onset and SSTs and SATs across the western and southernmost coastal areas, while weaker and fewer significant correlations are found between eastern SATs, SSTs, and freeze periods observed in the neighboring Greenland Sea. Autumn Greenland Blocking Index (GBI) values and the incidence of meridional circulation patterns have increased over the modern sea ice monitoring era. Increased anticyclonic blocking patterns promote poleward transport of warm air from lower latitudes and local warm air advection onshore from ocean-atmosphere sensible heat exchange through ice-free or thin ice-covered seas bordering the coastal stations. Temperature composites by years of extreme late freeze conditions, occurring since 2006 in Baffin Bay, reveal positive monthly SAT departures that often exceed one standard deviation from the 1981-2010 climate normal over coastal areas that exhibit a similar spatial pattern as the peak correlations.

Keywords: Arctic sea ice, Greenland, Greenland Blocking Index, surface air temperature, sea surface temperature

1. Introduction

Greenland coastal surface air temperature (SAT) records reveal predominantly increasing trends in monthly and seasonal means, variability, and extremes since the late 1970s/early 1980s (Hanna et al. 2012, 2014; Mernild et al. 2014). Over this time period during a strong phase of Arctic Amplification (Overland et al. 2015a), Arctic sea ice has dramatically declined – especially in early autumn (Perovich et al. 2015) – and its losses have been linked broadly to weather and climate anomalies in the Northern Hemisphere (e.g., Serreze and Barry 2011; Vihma 2014; Walsh 2014; Budikova and Chechi 2016). Several studies have associated local-to-pan-Arctic sea ice cover variability with Greenland ice sheet and outlet glacier behaviors (e.g., Rennermalm et al. 2009; Carr et al. 2013; Liu et al. 2016; McLeod and Mote 2016; Jensen et al. 2016). Robust sea-land ice linkages have been identified during summer as declining sea ice is related to melt conditions across south and west Greenland (Rennermalm et al. 2009; Liu et al. 2016; McLeod and Mote 2016).

Sea ice is one of many factors known to influence Greenland's coastal SAT signals and resultant environmental changes (e.g., Box 2002), although relatively few analyses have examined the interconnectivity of local sea ice, sea surface temperature (SST), SAT, and atmospheric circulation beyond the warm season months. Rogers et al. (1998) noted monthly SAT departures of 1-2 standard deviations below normal at weather stations situated along western Greenland and eastern Baffin Island spanning winter 1982 to autumn 1984. The authors associated this stint of cold coastal temperature anomalies with persistent SSTs of at least 0.5 standard deviations below normal coupled with extensive pack ice conditions and anomalous northerly surface winds across Baffin Bay and Davis

71 Strait. Over the 1958-1997 period, Deser et al. (2000) identified substantial winter
72 warming (cooling) SAT patterns adjacent to the island, especially to the east, collocated
73 with reduced (increased) areas of sea ice cover.

74 Since at least 2000, the Greenland region has been characterized by very different
75 synoptic sea-ice climate conditions from those seen in the early 1980s, including the
76 prevalence of anomalous autumn and winter anticyclonic regimes and rising coastal air
77 temperatures (Hanna et al. 2012; McLeod and Mote 2016) amidst negative cold-season sea
78 ice thickness anomalies (Nakamura et al. 2015). Simultaneously, since the mid-1990s
79 ocean heat transport towards southeast and west Greenland waters has been high (Buch et
80 al, 2004; Myers et al., 2007, 2009), resulting in increased sea temperatures propagating
81 northward into eastern Baffin Bay (Myers and Ribergaard, 2013; Ribergaard, 2014) and
82 likely affecting local sea ice conditions. Progressive delays in ice cover formation on Baffin
83 Bay and the Greenland Sea are also documented (Stroeve et al. 2014), which have lagged
84 ice-albedo feedback links to decreasing summer ice concentration that is coincident with
85 increases in solar heating and SST warming (Perovich et al. 2007). Increasingly persistent
86 blocking high pressure over Greenland is strongly linked with southerly meanders in the
87 polar jet stream (Hall et al. 2015; Overland et al. 2015b) and the North Atlantic Oscillation
88 (NAO)/Arctic Oscillation (AO) teleconnections (Woollings et al. 2010; Hanna et al. 2015,
89 2016). Increases in blocking, meridional flow patterns are associated with negative
90 NAO/AO phases and tend to promote mid-tropospheric ridging and southerly, warm air
91 advection across Greenland, leading to positive lower tropospheric/near-surface air
92 temperature anomalies that directly impact the local cryosphere (e.g., Box et al. 2012;
93 Fettweis et al. 2013; Hanna et al. 2013, 2014, 2016; Tedesco et al. 2016).

Motivated by the absence of recent physical-statistical studies analyzing potential links between Greenland coastal air temperatures and local sea ice variability during autumn, especially given the changing seasonality of the ice cover expressed in the freeze onset record, we analyze relationships in these variables from 1979-2014. Subsequently, we physically frame the statistical linkages found across the study period and during extreme autumn sea ice cases through a series of regional (Greenland-centric) to hemispheric-scale atmospheric circulation analyses. The paper is organized as follows: in Section 2, the data and methodology are described. In Section 3, trends in the SAT, SST, and sea ice data are explored and their relationships are assessed through correlation and composite techniques. The role of atmospheric circulation in linking sea ice conditions to SAT across portions of Greenland is evaluated in Section 4. A discussion and summary of the key findings are provided in Section 5.

2. Data and Methodology

2.1 Data

Annual Baffin Bay and Greenland Sea freeze dates, 1979-2014, are calculated from brightness temperatures obtained from a suite of passive microwave satellite sources, including the Scanning Multichannel Microwave Radiometer, the Special Sensor Microwave/Imager, and the Special Sensor Microwave Imager/Sounder. The data are quality-controlled and homogenized prior to being mapped and analyzed over a 25 km x 25 km polar stereographic grid. Processing procedures and the algorithm used to identify the freeze onset signal of each pixel are described in further detail by Markus et al. (2009). The annual freeze onset date falls within climatological autumn (SON) and signifies the

117 conclusion of that year's melt season, when the ocean surface temperature reaches the
118 freezing point and remains subfreezing through winter. Each freeze date time series
119 represents the long-term record of domain-averaged freeze conditions. The Baffin Bay and
120 Greenland Sea ice regions are identified in **Figure 1**, and follow the sea ice domains of
121 Markus et al. (2009; see their Figure 8). The Baffin Bay region also includes Davis Strait
122 and Labrador Sea, while the Greenland Sea region additionally spans the Iceland and
123 Irminger Seas. However, as the majority of the sea ice is found inside Baffin Bay and
124 Greenland Sea, we adopt similar domain names to Markus et al. (2009).

125 We select and analyze SAT data from locations along the eastern and western coasts
126 of Greenland for the months included within and surrounding the respective climatological
127 sea ice freeze onset periods, September – December, as well as the autumn and extended
128 autumn (SOND) seasons that span these months (**Figure 1**; **Table 1**). The SAT data
129 originate from two sources; weather stations maintained by the Danish Meteorological
130 Institute (DMI; Cappelen 2015), and gridded, model-derived output from ERA-Interim
131 (ERA-I) Reanalysis (Dee et al. 2011). Twelve DMI stations are selected for their proximity
132 to the coast and marginal seas of interest and due to the completeness of their monthly
133 records (>97% complete) across the modern satellite era. Three stations possessed one
134 month of missing data, Sisimiut (October 1998), Danmarkshavn (September, October
135 1981), and Ittoqqortoormiit (September, October 1981), which were subsequently filled
136 with the 36-year station monthly mean SAT. To enhance spatial coherence of coastal SAT
137 measurements, especially across the eastern Greenland coast, eight additional grid values
138 from ERA-I are selected. Prior to analysis, the reanalysis data are bilinearly interpolated
139 from their native ~0.7° latitude/longitude to a 5 x 5 km polar stereographic grid and

corrected for topographic errors in the reanalysis by using empirically-derived ice-sheet surface lapse rates, in a similar fashion to Hanna et al. (2005, 2011). These downscaled, orography-corrected SAT fields include the whole of Greenland and some surrounding portions of the ocean, not just the ice-sheet area, and have previously been used in positive-degree-day modeling of the Greenland Ice Sheet surface mass balance. Validation of the downscaled ERA-I temperature data is presented in Jowett et al. (2015), showing significant skill and low bias when compared with various in-situ Greenland SAT datasets. The monthly/seasonal SAT and sea ice time series are normalized with respect to their 1981-2010 means and standard deviations prior to being subjected to correlation and composite analyses (described in Section 2.2).

We supplement the freeze-SAT analyses with local SST analyses, including Baffin Bay, Labrador and Irminger Seas within the Baffin Bay ice domain, and the Greenland, Iceland and Irminger Seas over the Greenland Sea ice region to understand how the local SSTs relate to ice formation and coastal SATs over the autumn season. The SST product is gap free and based upon satellite observations from the Pathfinder Advanced Very High Resolution Radiometer (AVHRR) version 5.2 (Casey et al. 2010) and the Along-Track Scanning Radiometer (ATSR) Reprocessing for Climate (ARC) datasets (Embury et al. 2012). In addition, in-situ observations from the International Comprehensive Ocean-Atmosphere Data Set (ICOADS) version 2.5 have been included in the analysis (Woodruff et al. 2011). The observations have been merged using the interpolation method described in Høyer and She (2007) and Høyer et al. (2014) to generate a regional SST analysis, which is very similar to the climate data record described in Høyer and Karagali (2016). The data set thus consists of daily, gap free fields on a 0.05° resolution from 1982-2012. Validation

against independent in-situ observations have a standard deviation of about 0.5ºC and a bias of less than 0.1ºC (not shown). Local averages are calculated using this data set, where ice-covered areas were represented by an SST of -1.8ºC. To compare the sea ice, SAT, and SSTs in correlation analyses, the data are standardized by the 1982-2011 common period.

Studies of climatic and environmental changes across Greenland have often analyzed geopotential height (GPH) fields to identify synoptic-scale circulation mechanisms contributing to these changes. Here, we examine atmospheric flow patterns linking the autumn freeze onset and SAT time series through a number of disparate 500 hPa GPH analyses from 1979-2014. Aggregated monthly and seasonal GPH fields, derived from the NCEP/NCAR Reanalysis (Kalnay et al. 1996) are analyzed across Greenland to diagnose the climatological circulation over Greenland during the sea ice freeze onset era. GPH composites by respective extreme sea ice freeze years (described in Section 2.2) are also analyzed to evaluate relationships between sea ice and SAT. Lastly, daily mean GPH values (for all September through December days in the study period) are utilized to create a synoptic climatological classification of mid-tropospheric circulation patterns across the greater Greenland and immediately surrounding region of 55-85°N and 5-85°W (more details are provided in Section 2.2).

Monthly and seasonal values of the Greenland Blocking Index (GBI), NAO, and AO are subsequently analyzed to provide additional spatial (regional-to-hemispheric scale) and temporal (monthly/seasonal-averaged) atmospheric circulation context to the GPH analyses mentioned previously. The GBI represents the normalized 500 hPa mean GPH anomalies across Greenland, 60-80ºN, 20-80ºW (Fang 2004; Hanna et al. 2013, 2014, 2015, 2016). The AO is the initial EOF of 1000 hPa GPH anomalies northward of 20ºN (Thompson

and Wallace 1998). The NAO index version used here is the primary EOF of sea-level pressure from 20-80ºN and 40ºE-90ºW (Hurrell 1995).

2.2 Methodology

Trend, correlation, and composite analyses are applied to evaluate the sea ice and SAT data, and their statistical and physical associations through time. Prior to analysis, the normality of each dataset is assessed with a Shapiro-Wilk test. The majority of the data are normal justifying the usage of parametric statistics, including linear regression-based trends and Pearson product moment correlations. Here, trends represent the slope of the respective best-fit trend lines. Unless otherwise stated, linear trends are removed from all data prior to calculating correlation coefficients to emphasize the presence of interannual relationships. Statistical significance is assessed in the trend analyses and bivariate correlations with a two-tailed t-test and determined using a standard threshold of $p \leq 0.05$. Composite analyses, involving SAT and mid-tropospheric circulation data, are based on the Baffin Bay and Greenland Sea extreme freeze onset years that are ≥+1 standard deviation (late freeze) and ≤-1 standard deviation (early freeze) from their respective climatological mean freeze dates (listed in **Table 2** and shown in the bottom panel of **Figure 2**).

We also employ a synoptic climatological approach known as circulation pattern (CP) classification to identify the spectrum of Greenland's mid-tropospheric weather patterns that may further link sea ice and air temperature behaviors. This approach supplements our composite analyses by its ability to detect the prevalent, regional synoptic patterns within a large dataset (e.g., Key and Crane 1986). Synoptic climatologies involving Greenland have often focused on CP drivers of ice sheet melt (e.g., Mote 1998; Fettweis et

al. 2011; Belleflamme et al. 2013; Fettweis et al. 2013) rather than associations between adjacent sea ice and SAT measurements found across the island.

The classification method utilized here is k-means cluster analysis, which acts to minimize the distance of members grouped in the same cluster and maximize the distance of the centroids between each disparate cluster (Wilks 2011). In this study, each autumn day from 1979-2014 is categorized into one of the representative clusters, or CPs, that commonly occur over Greenland. An individual CP therefore reflects a composite mean of all days classified as that particular CP.

Prior to classification, a daily 500 hPa GPH spatial anomaly dataset is constructed from the raw GPH data by subtracting each day's domain mean height value from each grid point within the domain. Spatial anomalies are utilized to highlight the height field gradients, which dictate the strength of the flow aloft. Following a common pre-processing data reduction step in synoptic classification, the daily 500 GPH spatial anomaly data are subjected to an unrotated S-mode principal component analysis (PCA; Yarnal 1993). The PCA procedure serves to reduce the spatiotemporal GPH dataset into a smaller group of interpretable GPH patterns that cumulatively explain a high percentage of the total GPH variance and to eradicate multicollinearity between neighboring grid values. Application of the PCA technique on the GPH data yields 17 principal components (with eigenvalues of at least 1), which explain 98.54% of the original dataset variance. These principal components are introduced into the k-means clustering algorithm and each day is assigned membership to a specific cluster, or CP, based on similarities in spatial characteristics (i.e. flow shape and gradient). Ten CPs (k = 10) are identified in the analysis, which fall within the suggested CP retention limits when classifying at least 30 years of daily weather data

232 (Enke and Spekat 1997). Monthly CP frequency anomalies, with respect to their 1981-
233 2010 monthly average occurrence, are emphasized in the results.
234
235 **3. Statistical Links between SAT, SST, and Sea Ice**
236 *3.1 Trends*
237 **Figure 2** displays times series of freeze onset (top panel) and standardized
238 anomalies (bottom panel), relative to the 1981-2010 climate normal period, for Baffin Bay
239 and the Greenland Sea ice regions. Baffin Bay freeze onset ranges from day of year (DOY)
240 284 to 330 (i.e., October 11 – November 26), while Greenland Sea freeze onset tends to
241 occur earlier, spanning DOY 256 to 310 (i.e., September 13 to November 6). Both marginal
242 seas have witnessed substantial lengthening of the freeze season well into the core of
243 autumn. Since 1979, Baffin Bay's linear change is approximately +7.00 days decade^{-1} ($p <$
244 0.05), while Greenland Sea freeze onset change is roughly +8.20 days decade^{-1} ($p < 0.05$).
245 Delays in freeze onset appear related to upper-ocean mixed layer warming and SST
246 increases during summer (**Figure S1**). This summertime accumulation of heat has directly
247 affected autumn SST increases within the Baffin and Greenland ice domains, delaying
248 freeze onset conditions (**Figure S2**). Significant correlations between the raw (unadjusted)
249 time series ($r = +0.55$, $p < 0.05$) reflect a relatively synchronized shift from concurrent
250 early season ocean freezing prior to 2000 to a tendency toward anomalous late season
251 freeze onset over the last 15 autumns. Detrended correlations reveal a positive, but not
252 significant relationship ($r = +0.20$, $p = 0.25$) between the freeze observations that suggests
253 weak interannual associations despite linear trends of similar magnitude and sign. The

ongoing delays in ice cover formation mark substantial changes in the autumn sea-ice climatology surrounding Greenland.

Long-term trends in the east and west Greenland coastal air temperature records follow a similar sign to the neighboring sea-ice signals. Monthly trend magnitudes are relatively consistent (**Table 3**) and many demonstrate at least ~0.30ºC of warming per decade at the sampled coastal stations/grid points. Similar seasonal warming signals are identified in the DMI station-based datasets analyzed by Hanna et al. (2012; their Table 3c) for the 1981-2011 period. Consistent, significant warming in September is bookended by strong SAT increases during December, often reflecting a slight, yet sequential increase in the magnitude of the temperature anomalies in each individual autumn month (e.g., Aasiaat and Sisimiut). Extension of the SAT warming pattern into December could be related to lengthened periods of open water conditions (as diagnosed by near-coastal single pixel December SST values that have increased with time, especially southward from Upernavik along the western coast, not shown), sensible heat flux through young, thin ice cover (Maykut 1978), or a time-lagged signal from the sea ice-ocean heat flux feedback with increased Arctic sea-ice loss, especially west of Greenland (Overland et al. 2015b).

3.2 Correlations

Detrended correlation coefficients between the SATs and the disparate freeze onset datasets are presented in **Figures 3 and 4**. In-phase relationships between the SAT sites and nearby marginal seas are indicated by the spatial patterns of significant coefficients. For example, Baffin Bay freeze onset, well correlated with autumn Baffin Bay, Labrador Sea, and Irminger Sea SST variability (Table 4), is strongly and consistently linked to the

277 western/southern Greenland monthly and seasonal air temperatures (**Figure 3**). A
278 relatively uniform spatial pattern of statistically significant, positive correlations is
279 observed during October, preceding the 1979-2014 mean date of continuous, sub-freezing
280 temperatures on November 1, continuing with only slight magnitude decreases through
281 December. The highest, positive Baffin Bay sea-ice correlations with SAT occur at the
282 northwest stations, including Upernavik, Illulissat, and Aasiaat, during SON and SOND ($r > +0.60$, $p \leq 0.05$).

284 Upernavik temperature correlations show similar, robust associations with local
285 Baffin Bay SSTs as with freeze onset dates, suggesting that decreasing SSTs are mainly a
286 direct result of atmospheric cooling in this region (Table 4). Sea ice formation is delayed in
287 the eastern Baffin Bay due to the influence of warm Atlantic Water, which is transported
288 northward by the West Greenland Current (WGC) resulting in warmer SSTs on the
289 Greenland side of Baffin Bay before sea ice forms. More southerly stations also exhibit
290 strong SAT relationships with Baffin freeze dates and local SSTs (Table 4). However, these
291 are also more strongly influenced by the heat transport within the WGC, and the
292 correlations are slightly lower. Since the mid-1990s, the ocean heat transport within the
293 WGC has increased (Myers et al. 2007, 2009; Myers and Ribergaard, 2013), which may
294 have weakened the strong relationship between SATs and SSTs in the area.

295 Associations between Greenland Sea ice and SSTs and east coast air temperatures
296 are generally positive but weaker, with fewer significant correlations relative to the
297 western flank of the island (**Figure 4** and **Table 4**). This may be due to local oceanographic
298 differences as Baffin Bay ice forms and is influenced predominantly by local ocean-
299 atmosphere interactions, while the Greenland Sea ice formation is a product of both local

processes and southward Arctic sea ice flux through Fram Strait (Kwok et al. 2004). This east-west difference may also partially result from closer station proximity to the ice sheet coupled with steeper east coast topography and stronger resultant katabatic winds, which inhibit the maritime influence on adjacent coastal SATs (Noël et al. 2014). These correlations are strongest during October, overlapping the climatological freeze onset occurring early in the month, as well as December and the autumn season aggregations, particularly along the southeastern coast at EG 4, EG 5, and Tasiilaq. In analyses of each ice domain, we observe significant, lagged temperature responses to freeze onset in December, but cross-island ice-SAT teleconnections are generally weak, especially spanning the northernmost coastal sites.

The correlation analysis clearly reveals, that the hydrographic surface conditions in northeast Greenland waters (Greenland Sea and Iceland Sea), are quite different from those in southeast and west Greenland waters (Irminger Sea, Labrador Sea, and Baffin Bay) (**Table 4)**. The near-surface currents are cyclonic, highly topographically steered, and strongest at the rim of the ocean basins (Jakobsen et al., 2003). The East Greenland Current (EGC) carries cold, low-salinity Polar water and sea ice southward, which characterizes northeast Greenland waters. Much warmer and saltier Irminger waters join the EGC in the northern part of the Irminger Sea, resulting in warmer hydrographic conditions off southeast and west Greenland including eastern Baffin Bay (Buch et al., 2004; Ribergaard, 2013).

3.3 SAT Composite Analyses

Monthly and seasonal SAT behaviors during anomalously late and early freeze conditions are investigated by marginal sea. Late ice formation across Baffin Bay tends to coincide with widespread, above-average coastal SATs (**Figure 5**). Months of open water (September and October) are linked with some spatial SAT similarities as shown by positive temperature anomalies situated along western and southern Greenland, including some sites on the southeastern coast. Temperature anomalies weaken during November as late freezes occur toward the middle-to-end of the month, then strengthen in December as thin ice cover develops, with many southern latitude locations exhibiting temperature departures exceeding one standard deviation (e.g., EG 4-6 and Tasiilaq). Early freeze onsets, clustered during mid-October, promote below-normal monthly SATs (of similar magnitude, but opposite sign from late freeze years), especially along the west coast as the cold SSTs allow first-year ice formation earlier in the season (**Figure 6**). Perhaps not surprisingly, the largest positive SAT differences (late – early years) are seen along the western, southern, and southeastern portions of coastal Greenland where strong temperature responses to extreme sea ice behaviors are noted (**Figure S3**).

Late Greenland Sea freeze onsets correspond with relatively weak temperature responses, except during December when strong, positive east coast temperature departures (more than one standard deviation) are found, as is similar to late onset ice cover in Baffin Bay (**Figure S4**). Negative temperature anomalies are found with early ice formation (**Figure S5**), but the SAT magnitudes are generally weaker in September-November compared to the Baffin Bay early freeze findings. The strongest SAT differences between extreme Greenland Sea ice freeze scenarios are observed during December and SOND, but restricted to the east coast of the island (**Figure S6**).

4. Associations between SAT and Sea Ice through Atmospheric Circulation

4.1 Trends and Correlations

The timing of Baffin Bay and Greenland Sea ice formation appears to play a role in the variability of Greenland's coastal air temperatures during autumn. We investigate associations between the two variables here through analyses of different atmospheric circulation variables across the study period. Monthly and seasonal mean 500 hPa GPH fields show an upper-level trough west of Greenland stretching across Baffin Bay that sags southward and deepens throughout the autumn months, transitioning from more westerly to southwesterly flow onto the western coast (**Figure 7**). GBI linear trend analyses for autumn, presented in **Figure 7,** reveal positive trends in October – December, especially during October (statistically significant increase) and December, which supports the findings of Hanna et al. (2016) over the 1981-2010 normal period. In a long-term view, increases in the GBI suggest that greater occurrences of high-pressure blocking synoptic patterns could be taking place over Greenland, which may act to increasingly 1) advect above-freezing air masses northward from lower latitudes to delay sea ice growth, and 2) transport warm air off the local, open-ocean or young ice surfaces, which are becoming more common later in the autumn, toward the coast to directly impact SATs. Year-to-year GBI fluctuations are also related (in-phase) to the interannual variability of the coastal SATs and onset of sea ice freeze conditions, especially along the west coast (**Figure 8**). These relationships suggest that changes in regional winds (inferred by GBI anomalies) influence SATs each season depending on the timing of freeze conditions.

The circulation patterns (CPs) identified through k-means cluster analysis are presented in **Figure 9**. Each composite CP represents a typical synoptic regime that occurs anywhere from ~2 – 4 days per month and ~7 – 14 days per season, across the Greenland region (**Table S1**). Correlations between the CP frequencies and GBI are calculated to assess relationships between within-month/season synoptic variability and the monthly/seasonal GBI conditions (**Table 5**).

Significant correlations between the frequencies of CPs 3, 9, and 10 and the GBI are discussed here. CP 3, a meridional pattern with a relatively weak west-east height gradient, is positively and significantly correlated with the GBI in all months (except November) and seasonally, while CP 10, exhibiting southwesterly flow across Greenland, is positively and significantly correlated with the GBI in November, December, and for the whole autumn season. The incidence of synoptic patterns yielding onshore flow from the southerly (CP3)/southwesterly (CP 10) direction coincides with interannual oscillations in autumn GBI values, which are connected to variations in the coastal SATs. CP 9 possesses a weak north-south gradient across much of Greenland that strengthens south and east across the North Atlantic and is significantly anti-correlated with the GBI, except during October when there is no apparent relationship. Significant anti-correlations also occur between these three CPs and the regional-scale NAO and hemispheric-scale AO teleconnections, respectively (**Tables S2 and S3**). Positive (negative) values of these broader-scale atmospheric circulation indices tend to coincide with relatively zonal (meridional) flow across Greenland, further supporting these sea ice-SAT linkages.

4.2 Atmospheric Circulation Composite Analyses

390 Composite 500 hPa GPH plots by late – early Baffin Bay freeze years are shown in
391 **Figure 10**. Positive height anomalies over Greenland occur for all autumn months and the
392 season as a whole. These differences are strongest during October and December, similar
393 to the SAT peak response, as height field anomalies largely exceed +100 m across the
394 island. GBI composites are similarly maximized during these months (October GBI = +2.27
395 and December GBI = +1.88) as diminished Baffin Bay sea ice cover has been linked with
396 increased lower tropospheric temperatures and mid-level heights during October and
397 December (Overland et al. 2015b), shortly after the onset of freeze conditions. Relative to
398 Baffin Bay, mid-tropospheric GPH anomalies are substantially weaker during extreme year
399 composites of Greenland Sea ice conditions, perhaps due to earlier extreme freeze timing
400 across the marginal sea in both late and early cases. Despite weaker flow anomalies, it is
401 worth noting that the height field is considerably above normal (≥+60 m) across the ice
402 domain and island during December (**Figure S7**).
403 The occurrence of intra-monthly/seasonal synoptic regimes by extreme freeze years
404 is similarly shown in **Table 6** for Baffin Bay. In October, nearly 6 more days of meridional
405 flow (i.e., CP 3 occurrence) occur during late versus early freeze years, and positive
406 occurrence anomalies of lesser magnitude (~+2 days) are also found in September and
407 seasonally. Meridional CPs 7 and 8 also exhibit slight positive anomalies (~+1 day) during
408 December, while weak gradients/zonal flow patterns show negative differences of at least
409 two days within the month (e.g., CPs 4 and 9). Greenland Sea ice freeze extreme
410 composites similarly show an increased incidence of meridional CPs 2, 7, and 8 during
411 December (**Table S4**). Overall, composite flow analyses by marginal sea freeze anomalies
412 (late – early years) show tendencies toward more meridional synoptic patterns in the

months of highest GBI values. This increased occurrence of wavier, blocking-type flow provides evidence of a physical mechanism by which warmer air over the ice-free ocean and from lower latitudes is directed onto coastal areas thereby influencing changes in SATs.

5. Discussion and Conclusions

In this study, strong autumn season associations between coastal Greenland SATs, SSTs, and neighboring sea ice conditions are identified and physically linked through several analyses of atmospheric circulation patterns. Initially, a high degree of co-variability is recognized through bivariate correlations between the Baffin Bay freeze onset dates and SATs extending along the southern and western coastal margins, whereas much weaker, less significant signals are identified between Greenland Sea ice and adjacent east coast SATs. Increased oceanic heat transfer along the western Greenland coast by the WGC during the last two decades (Myers et al. 2007, 2009; Myers and Ribergaard 2013) has likely played a role in delaying Baffin Bay ice formation and strengthening freeze onset-SAT relationships in the region. Baffin Bay-SAT relationships are especially pronounced in anomalously late (early) freeze years, which are found after (before) 2000, and frequently coincide with SATs above (below) one standard deviation from the 1981-2010 SAT climatology.

The long-term and extreme Baffin Bay ice cover linkages to autumn SAT signals identified in the analyses are influenced by variability of the geopotential height field across Greenland. Steffen and Box (2001) note a seasonal shift in the shape of climatological upper-level flow from a zonal pattern in summer to a meridional one in

436 winter atop the ice sheet. As shown in Section 4.1, the 500 hPa mean circulation
437 strengthens and becomes slightly more meridional as autumn progresses. Further, the
438 autumn GPHs over Greenland have shown a linear increase since 1979, especially during
439 October and December as corroborated by Hanna et al (2016) for the most recent 1981-
440 2010 normal period. GPH field amplification is associated with increasingly
441 anticyclonic/blocking flow over the island (e.g., Hanna et al. 2016) that dynamically ushers
442 warm and moist air from lower latitudes across Baffin Bay and the neighboring west coast
443 of Greenland (Dufour et al. 2016). Poleward warm air advection of above-freezing air acts
444 to also delay Baffin Bay sea ice formation and increases the incidence of open water near
445 coastal areas, which amplifies local air temperatures (at least until ice cover thickens)
446 through a positive feedback (Box 2002). Air-sea processes over the west coast of the island
447 also likely have a strong local component as sensible heat released through young, thin sea
448 ice found in Labrador Sea and Baffin Bay is advected onshore more frequently when
449 Greenland blocking patterns are present.

450 Recent, anomalous meridionality has been identified in the cold-season North
451 Atlantic polar jet stream (e.g., Francis and Vavrus 2015; Francis and Skific 2015; Hall et al.
452 2015). This is coincident with rising GBI values, shown here to co-vary interannually with
453 sea ice and coastal SATs from October to December and during autumn. Significant,
454 positive correlations are found between the incidence of ridging/meridional circulation
455 across Baffin Bay and the autumn GBI values. Links between wavier upper-level flow
456 frequencies and the October AO and NAO (prior to typical continuous freeze conditions on
457 Baffin Bay) and the December AO (as seasonal sea ice cover continually forms, thickens,
458 and expands throughout the neighboring seas) are also noted. Hanna et al. (2016) found

459 positive GPH anomalies across the Arctic (at the 300, 500, 700, 850 hPa levels), reminiscent
460 of a negative AO phase, during extreme, positive December GBI conditions. The authors
461 also identified positive correlations between the GBI and SATs surrounding Greenland in
462 this month dating back to the late-19th century. Positive lower tropospheric temperature
463 and mid-level circulation anomalies observed around greater Greenland during several
464 Decembers since 2007 have been loosely associated with autumn sea ice losses (e.g.,
465 Overland and Wang 2015; Overland et al. 2015b), and therefore may in part reflect an
466 ongoing lagged response to extreme late freeze onset or perhaps increased ocean-
467 atmosphere heat flux through a slowly forming ice pack. Regardless of the driver(s) of
468 regional height field amplification, our study shows that the prevalence of autumn blocking
469 over Greenland since the 1980s represents a robust mechanism that modulates the
470 interannual strength of the sea ice-SAT relationships and the magnitude of SAT anomalies
471 in extreme freeze years, especially on the western coast.

472 Should the Arctic sea ice melt season continue its present course of lengthening
473 (Parkinson 2014; Stroeve et al. 2014), increased periods of open-water conditions will
474 likely continue to alter the climatology of coastal observations in Greenland and other
475 portions of the Arctic. The magnitude of long-term SAT changes, embedded with short-
476 term extremes, will probably be further influenced by sea-ice interactions with regional-to-
477 hemispheric atmospheric circulation patterns as well as other confounding factors of
478 Greenland climate variability, such as Atlantic and Pacific SST fluctuations (e.g., Chylek et al.
479 2012; Ding et al. 2014).
480

Acknowledgements: The editor and reviewers are thanked for their constructive comments, which helped improve the manuscript. Special thanks to David McCutcheon (Department of Geography, University of Sheffield) for his assistance in drafting Figure 1. The AO dataset is obtained through the Climate Prediction Center webpage (http://www.cpc.ncep.noaa.gov/products/precip/CWlink/daily_ao_index/teleconnections.shtml), and NAO data may be found on the NCAR Climate Data Guide website (https://climatedataguide.ucar.edu/climate-data/hurrell-north-atlantic-oscillation-nao-index-pc-based). GBI data can be accessed from: https://www.sheffield.ac.uk/geography/staff/hanna_edward/gbi. NCEP/NCAR Reanalysis data are obtained from http://www.esrl.noaa.gov/psd/data/gridded/data.ncep.reanalysis.html.

EH and RJH acknowledge support from the University of Sheffield's Project Sunshine.

References

Belleflamme A, Fettweis X, Lang C, Erpicum M (2013) Current and future atmospheric circulation of 500 hPa over Greenland simulated by CMIP3 and CMIP5 global models. *Climate Dynamics* 41: 2061-2080. doi:10.1007/s00382-012-1538-2.

Box JE (2002) Survey of Greenland instrumental temperature records: 1873-2001. *International Journal of Climatology* 22: 1829-1847. doi:10.1002/joc.852.

Box JE, Fettweis X, Stroeve JC, Tedesco M, Hall DK, Steffen K (2012) Greenland ice sheet albedo feedback: thermodynamics and atmospheric drivers. *The Cryosphere* 6: 821-839. doi:10.5194/tc-6-821-2012.

Buch E, Pedersen SA, Ribergaard MH (2004) Ecosystem variability in West Greenland waters. *Journal of Northwest Atlantic Fishery Science* 34, 13-28. doi:10.2960/J.v34.m479.

Budikova D, Chechi L (2016) Arctic sea ice and warm season North American extreme surface air temperatures. *Climate Research* 67: 15-29. doi:10.3354/cr01349.

Cappelen J (2015) Greenland – DMI historical climate data collection 1873-2014 – with Danish abstracts. Technical Report No 15-04, DMI, Copenhagen, Denmark.

Carr JR, Vieli A, Stokes C (2013) Influence of sea ice decline, atmosphere warming, and glacier width on marine-terminating outlet glacier behavior in northwest Greenland at seasonal to interannual time scales. *Journal of Geophysical Research - Earth Surface* 118: 1210-1226. doi:10.1022/jgrf.20088.

514 Casey, KS, Brandon TB, Cornillon P, Evans R (2010) The past, present, and future of the
515 AVHRR Pathfinder SST program. *In Oceanography from space* (pp. 273-287). Springer
516 Netherlands.

517 Chylek P, Folland C, Frankcombe L, Dijkstra H, Lesins G, Dubey M (2012) Greenland ice core
518 evidence for spatial and temporal variability of the Atlantic Multidecadal Oscillation.
519 *Geophysical Research Letters* 39: L09705. doi:10.1029/2012GL051241, 2012.

520 Dee DP, Uppala SM, Simmons AJ, Berrisford P, Poli P, Kobayashi S, Andrae U, Balmaseda
521 MA, Balsamo G, Bauer P, Bechtold P, Beljaars ACM, van de Berg L, Bidlot J, Bormann N,
522 Delsol C, Dragani R, Fuentes M, Geer AJ, Haimberger L, Healy SB, Hersbach H, Hólm
523 EV, Isaksen L, Kållberg P, Köhler M, Matricardi M, McNally AP, Monge-Sanz BM,
524 Morcrette J-J, Park BK, Peubey C, de Rosnay P, Tavolato C, Thépaut J-N, Vitart F (2011)
525 The ERA-Interim reanalysis: configuration and performance of the data assimilation
526 system. *Quarterly Journal of the Royal Meteorological Society* 137: 553–597.
527 doi:10.1002/qj.828.

528 Deser C, Walsh JE, Timlin MS (2000) Arctic sea ice variability in the context of recent
529 atmospheric circulation trends. *Journal of Climate* 13: 617-633.

530 Ding Q, Wallace JM, Battisti DS, Steig EJ, Gallant AJE, Kim H-J, Geng L (2014) Tropical forcing
531 of the recent rapid Arctic warming in northeastern Canada and Greenland. *Nature*
532 509: 209-213. doi:10.1038/nature13260.

533 Dufour A, Zolina O, Gulev S (2016) Atmospheric moisture transport to the Arctic:
534 assessment of reanalyses and analysis of transport components. *Journal of Climate*, in
535 press. doi:10.1175/JCLI-D-15-0559.

536 Embury O, Merchant CJ, Corlett GK (2012) A reprocessing for climate of sea surface
537 temperature from the along-track scanning radiometers: Initial validation, accounting
538 for skin and diurnal variability effects. *Remote Sensing of Environment*, 116, 62-78.
539 Enke W, Spekat A (1997) Downscaling climate model outputs into local and regional
540 weather elements by classification and regression. *Climate Research* 8: 195-207.
541 Fang, Z.-F. (2004) Statistical relationship between the Northern Hemisphere sea ice and
542 atmospheric circulation during wintertime. Observation, Theory and Modeling of
543 Atmospheric Variability, X. Zhu, Ed., World Scientific, 131–141.
544 Fettweis X, Mabille G, Erpicum M, Nicolay S, Van den Broeke M (2011) The 1958-2009
545 Greenland ice sheet surface melt and the mid-tropospheric atmospheric circulation.
546 *Climate Dynamics* 36: 139-159. doi:10.1007/s00382-010-0772-8.
547 Fettweis X, Hanna E, Lang C, Belleflamme A, Erpicum M, Gallée H (2013) Important role of
548 the mid-tropospheric atmospheric circulation in the recent surface melt increase over
549 the Greenland ice sheet. *Cryosphere* 7: 241–248.
550 Francis J, Skific N (2015) Evidence linking rapid Arctic warming to mid-latitude weather
551 patterns. *Philosophical Transactions of the Royal Society A* 373: 20140170.
552 doi:10.1098/rsta.2014.0170.
553 Francis JA, Vavrus SJ (2015) Evidence for a wavier jet stream in response to rapid Arctic
554 warming. *Environmental Research Letters* 10: 014005. doi:10.1088/1748-
555 9326/10/1/014005.
556 Hall R, Erdélyi R, Hanna E, Jones JM, Scaife AA (2015) Drivers of North Atlantic Polar Front
557 jet stream variability. *International Journal of Climatology* 35: 1697-1720.
558 doi:10.1002/joc.4121.

559 Hanna E, Huybrechts P, Janssens I, Cappelen J, Steffen K, Stephens A (2005) Runoff and
560 mass balance of the Greenland Ice Sheet: 1958-2003. *Journal of Geophysical Research-*
561 *Atmospheres*, 110: D13108. doi:10.1029/2004JD005641.
562 Hanna E, Huybrechts P, Cappelen J, Steffen K, Bales RC, Burgess E, McConnell JR, Steffensen
563 JP, Van den Broeke M, Wake L, Bigg G, Savas D (2011) Greenland Ice Sheet surface
564 mass balance 1870 to 2010 based on Twentieth Century Reanalysis, and links with
565 global climate forcing. *Journal of Geophysical Research* 116: D24121.
566 doi:10.1029/2011JD016387.
567 Hanna E, Mernild SH, Cappelen J, Steffen K (2012) Recent warming in Greenland in a long-
568 term instrumental (1881-2012) climatic context: I. Evaluation of surface air
569 temperature records. *Environmental Research Letters* 7: 1-15. doi:10.1088/1748-
570 9326/7/4/045404.
571 Hanna E, Jones JM, Cappelen J, Mernild SH, Wood L, Steffen K, Huybrechts P (2013) The
572 influence of North Atlantic atmospheric and oceanic forcing effects on 1900–2010
573 Greenland summer climate and ice melt/runoff. *International Journal of Climatology*,
574 33: 862–880. doi: 10.1002/joc.3475.
575 Hanna E, Fettweis X, Mernild SH, Cappelen J, Ribergaard MH, Shuman CA, Steffen K, Wood
576 L, Mote T (2014) Atmospheric and oceanic climate forcing of the exceptional
577 Greenland ice sheet surface melt in summer 2012. *International Journal of*
578 *Climatology* 34: 1022-1037. doi:10.1002/joc.3743.
579 Hanna E, Cropper TE, Jones PD, Scaife AA, Allen R (2015) Recent summer asymmetric
580 changes in the NAO (a marked summer decline and increased winter variability) and

associated changes in the AO and Greenland Blocking Index. *International Journal of Climatology* 35: 2540-2554. doi:10.1002/joc.4157.

Hanna E, Cropper TE, Hall RJ, Cappelen J (2016) Greenland Blocking Index 1851-2015: a regional climate change signal. *International Journal of Climatology*, in press. doi:10.1002/joc.4673.

Høyer JL, She J (2007) Optimal interpolation of sea surface temperature for the North Sea and Baltic Sea. *Journal of Marine Systems*, 65(1), 176-189.

Høyer JL, Le Borgne P, Eastwood S (2014) A bias correction method for Arctic satellite sea surface temperature observations. *Remote Sensing of Environment*, 146, 201-213.

Høyer JL, Karagali I (2016) Sea surface temperature climate data record for the North Sea and Baltic Sea. *Journal of Climate* 29: 2529-2541. doi:10.1175/JCLI-D-15-0663.1.

Hurrell JW. 1995. Decadal trends in the North Atlantic oscillation: regional temperatures and precipitation. *Science* 269: 676–679.

Jakobsen PK, Ribergaard MH, Quadfasel D, Schmith T, Hughes CW (2003) The near surface circulation in the Northern North Atlantic as inferred from Lagrangian drifters: variability from the mesoscale to interannual. *Journal of Geophysical Research* 108 (C8), 3251. doi:10.1029/2002JC001554.

Jensen TS, Box JE, Hvidberg CS (2016) A sensitivity study of annual area change for Greenland ice sheet marine terminating outlet glaciers: 1999–2013. *Journal of Glaciology* 62: 72-81. doi:10.1017/ jog.2016.12.

Jowett AE, Hanna E, Ng F, Huybrechts P, Janssens I (2015) A new spatially and temporally variable sigma parameter in degree-day melt modelling of the Greenland Ice Sheet 1870–2013. *The Cryosphere Discussions* 9: 5327-5371. doi:10.5194/tcd-9-5327-2015.

604 Kalnay E, Kanamitsu M, Kistler R, Collins W, Deaven D, Gandin L, Iredell M, Saha S, White G,
605 Woollen J, Zhu Y, Chelliah M, Ebisuzaki W, Higgins W, Janowiak J, Mo KC, Ropelewski C,
606 Wang J, Leetmaa A, Reynolds R, Jenne R, Joseph D (1996) The NCEP/NCAR 40-year
607 reanalysis project. *Bulletin of the American Meteorological Society* 77: 437-471.
608 Key J, Crane RG (1986) A comparison of synoptic classification schemes based on 'objective'
609 procedures. *Journal of Climatology* 6: 375-388.
610 Kwok R, Cunningham GF, Pang SS (2004) Fram Strait sea ice outflow. *Journal of*
611 *Geophysical Research – Oceans* 109, C01009. doi:19.1029/2003JC001785.
612 Liu J, Chen Z, Francis J, Song M, Mote T, Hu Y (2016) Has Arctic sea-ice loss contributed to
613 increased surface melting of the Greenland ice sheet? *Journal of Climate*, in press.
614 doi:10.1175/JCLI-D-15-0391.
615 Markus T, Stroeve JC, Miller J (2009) Recent changes in Arctic sea ice melt onset, freezeup,
616 and melt season length. *Journal of Geophysical Research* 114**:** C12024.
617 doi:10.1029/2009JC005436.
618 Maykut GA (1978) Energy exchange over young sea ice in the Central Arctic. *Journal of*
619 *Geophysical Research* 83: 3646-3658.
620 McLeod JT, Mote TL (2016) Linking interannual variability in extreme Greenland blocking
621 episodes to the recent increase in summer melting across the Greenland ice sheet.
622 *International Journal of Climatology* 36: 1484-1499. doi:10.1002/joc.4440.
623 Mernild SH, Hanna E, Yde JC, Cappelen J, Malmros JK (2014) Coastal Greenland air
624 temperature extremes and trends 1890-2010: annual and monthly analysis.
625 *International Journal of Climatology* 34: 1472-1487. doi:10.1002/joc.3777.

626 Mote TL (1998) Mid-tropospheric circulation and surface melt on the Greenland ice sheet.
627 Part II: Synoptic climatology. *International Journal of Climatology* 18: 131-145.
628 Myers PG, Kulan N, Ribergaard MH (2007) Irminger Water variability in the West
629 Greenland Current. *Geophysical Research Letters* 34, L17601.
630 doi:10.1029/2007GL030419.
631 Myers PG, Donnelly C, Ribergaard, MH (2009) Structure and Variability of the West
632 Greenland Current in Summer Derived From 6 Repeat Standard Sections. *Progress in*
633 *Oceanography* 80, 93-112. doi:10.1016/j.pocean.2008.12.003
634 Myers PG, Ribergaard MH (2013) Warming of the Polar Water Layer in Disko Bay and
635 Potential Impact on Jakobshavn Isbrae. *Journal of Physical Oceanography* 43, 2629-
636 2640. doi:10.1175/JPO-D-12-051.1.
637 Nakamura T, Yamazaki K, Iwamoto K, Honda M, Miyoshi Y, Ogawa Y, Ukita J (2015) A
638 negative phase shift of the winter AO/NAO due to the recent Arctic sea-ice reduction in
639 late autumn. *Journal of Geophysical Research – Atmospheres* 120: 3209-3227.
640 doi:10.1002/2014JD022848.
641 Noël B, Fettweis X, van de Berg W, van den Broeke M, Erpicum M (2014) Sensitivity of
642 Greenland Ice Sheet surface mass balance to perturbations in sea surface temperature
643 and sea ice cover: a study with the regional climate model MAR. *Cryosphere* 8: 1871 –
644 1883. doi: 10.5194/tc-8-1871-2014.
645 Overland JE, Wang M (2015) Increased variability in the early winter subarctic North
646 American atmospheric circulation. *Journal of Climate* 28: 7297-7305. doi:
647 10.1175/JCLI-D-15-0395.1.

Overland J, Hanna E, Hanssen-Bauer I, Kim S-J, Walsh JE, Wang M, Bhatt US, Thoman RL (2015a) Surface air temperature [in Arctic Report Card 2015]. http://www.arctic.noaa.gov/reportcard.

Overland J, Francis JA, Hall R, Hanna E, Kim S-J, Vihma T (2015b) The melting Arctic and midlatitude weather patterns: Are they connected? *Journal of Climate* 28: 7917-7932. doi: 10.1175/JCLI-D-14-00822.1.

Parkinson CL (2014) Spatially mapped reductions in the length of the Arctic sea ice season. *Geophysical Research Letters* 41: 4316-4322. doi:10.1002/2014GL060434.

Perovich DK, Light B, Eicken H, Jones KF, Runciman K, Nghiem SV (2007) Increasing solar heating of the Arctic Ocean and adjacent seas, 1979-2005: Attribution and role in the ice-albedo feedback. *Geophysical Research Letters* 34, L19505. doi:10.1029/2007/GL031480.

Perovich D, Meier W, Tschudi M, Farrell S, Gerland S, Hendricks S (2015) Sea ice [in Arctic Report Card 2015]. http://www.arctic.noaa.gov/reportcard.

Rennermalm A, Smith L, Stroeve J, Chu V (2009) Does sea ice influence Greenland ice sheet surface-melt? *Environmental Research Letters* 4: 1-7. doi:10.1088/1748-9326/4/2/024001.

Ribergaard, MH (2014) Oceanographic Investigations off West Greenland 2013. *NAFO Scientific Council Documents* 14/001.

Rogers JC, Wang C-C, McHugh MJ (1998) Persistent cold climatic episodes around Greenland and Baffin Island: Links to decadal-scale sea surface temperature anomalies. *Geophysical Research Letters* 25: 3971-3974.

670 Serreze MC, Barry RG (2011) Processes and impacts of Arctic amplification: A research
671 synthesis. *Global and Planetary Change* 77: 85-96.
672 doi:10.1016/j.glopacha.2011.03.004.
673 Steffen K, Box J (2001) Surface climatology of the Greenland ice sheet: Greenland Climate
674 Network 1995-1999. Journal of Geophysical Research 106: 33951-33964.
675 Stroeve JC, Markus T, Boisvert L, Miller J, Barrett A (2014) Changes in Arctic melt season
676 and implications for sea ice loss. *Geophysical Research Letters* 41: 1216–1225.
677 doi:10.1002/2013GL058951.
678 Tedesco M, Mote T, Fettweis X, Hanna E, Jeyaratnam J, Booth JF, Datta R, Briggs K (2016)
679 Arctic cut-off high drives the poleward shift of a new Greenland melting record. *Nature*
680 *Communications* 7:11723. doi: 10.1038/ncomms11723.
681 Thompson DWJ, Wallace JM (1998) The Arctic oscillation signature in the wintertime
682 geopotential height and temperature fields. *Geophysical Research Letters* 25: 1297–
683 1300.
684 Vihma T (2014) Effects of Arctic sea ice decline on weather and climate: A review. *Surveys*
685 *in Geophysics* 35: 1175-1214. doi:10.1007/s10712-014-9284-0.
686 Walsh JE (2014) Intensified warming of the Arctic: Causes and impacts on middle latitudes.
687 *Global and Planetary Change* 117: 52-63. doi:10.1016/j.gloplacha.2014.03.003.
688 Wilks DS (2011) *Statistical methods in the Atmospheric Sciences*, 3rd edition. Academic
689 Press, Oxford, UK.
690 Woodruff SD, Worley SJ, Lubker SJ, Ji Z, Freeman JE, Berry DI, Brohan P, Kent EC, Reynolds
691 RW, Smoth SR, Wilkinson C (2011) ICOADS Release 2.5: extensions and enhancements

692 to the surface marine meteorological archive. *International Journal of Climatology*,
693 31(7), 951-967.
694 Woollings T, Hannachi A, Hoskins B, Turner A (2010) A regime view of the North Atlantic
695 Oscillation and its response to anthropogenic forcing. *Journal of Climate* 23: 1291-
696 1307.
697 Yarnal B (1993) *Synoptic Climatology in Environmental Analysis: A primer*. Belhaven Press,
698 195 pp.
699
700

Tables

Station/Grid Point Name	Data Source	WMO Code	Lat (°N)	Lon (°W)	Data Record
Western Greenland (WG) SAT					
WG1	ERA-I	-	75.00	57.10	1979-2014
Upernavik	DMI	04211	72.78	56.13	1979-2014
Illulissat	DMI	04221	69.23	51.07	1979-2014
Aasiaat	DMI	04220	68.70	52.75	1979-2014
Kangerlussuaq	DMI	04231	67.17	50.70	1979-2014
Sisimiut	DMI	04234	66.92	53.67	1979-2014
Nuuk	DMI	04250	64.17	51.75	1979-2014
Paamiut	DMI	04260	62.00	49.67	1979-2014
Narsarsuaq	DMI	04270	61.17	45.42	1979-2014
Qaqortoq	DMI	04272	60.72	46.05	1979-2014
Eastern Greenland (EG) SAT					
Danmarkshavn	DMI	04320	76.77	18.67	1979-2014
EG1	ERA-I	-	74.21	19.97	1979-2014
EG2	ERA-I	-	72.31	26.04	1979-2014
Ittoqqortoormiit	DMI	04339	70.48	21.95	1979-2014
EG3	ERA-I	-	68.92	28.28	1979-2014
EG4	ERA-I	-	67.91	32.44	1979-2014
EG5	ERA-I	-	66.49	33.95	1979-2014
Tasiilaq	DMI	04360	65.60	37.63	1979-2014
EG6	ERA-I	-	64.16	40.98	1979-2014
EG7	ERA-I	-	61.68	41.98	1979-2014

Table 1. Details of the coastal Greenland surface air temperature (SAT) datasets.

Sea Ice Domain	Earliest Freeze DOY (Date)	Latest Freeze DOY (Date)	Freeze Mean (Day)	Freeze SD	Late Freeze DOY* (Dates)	Early Freeze DOY** (Dates)
Baffin Bay	283.75 (Oct 11, 1986)	329.76 (Nov 26, 2010)	305.19 (Nov 1)	10.17	315.67 (Nov 12, 2006) 318.00 (Nov 14, 2009) 319.32 (Nov 15, 2002) 322.16 (Nov 17, 2012) 329.76 (Nov 26, 2010)	283.75 (Oct 11, 1986) 287.11 (Oct 14, 1996) 290.06 (Oct 17, 1983) 290.71 (Oct 18, 1982) 291.36 (Oct 18, 1990)
Greenland Sea	256.12 (Sept 13, 1983)	309.51 (Nov 6, 2002)	277.85 (Oct 4)	14.06	295.24 (Oct 21, 2008) 298.48 (Oct 25, 2001) 298.76 (Oct 25, 2012) 299.92 (Oct 27, 2014) 300.42 (Oct 26, 1984) 300.89 (Oct 27, 2009) 309.51 (Nov 6, 2002)	256.12 (Sept 13, 1983) 258.43 (Sept 15. 1981) 261.04 (Sept 18, 1987) 261.52 (Sept 19, 1979) 262.01 (Sept 19, 1994) 263.21 (Sept 19, 1992)

*≥+1 SD from freeze mean

**≤-1 SD from freeze mean

Table 2. Baffin Bay and East Greenland Sea freeze onset climatology, 1979-2014. Day of year (DOY) and date are shown where individual years are identified. Dates in parentheses represent the beginning of continuous mean freeze conditions for the given year, rounded to the nearest day. Freeze mean and standard deviation (SD) represent the 1981-2010 period, and are used to construct the normalized freeze anomalies displayed in Figure 2. The freeze mean reflects the average freeze day on a non-leap year.

716

Station/Grid Point Name	Sept	Oct	Nov	Dec	SON	SOND
WG1	+0.26	-0.30	**-1.44**	-0.90	-0.49	**-0.59**
Upernavik	+0.34	+0.50	+0.78	**+1.84**	**+0.54**	**+0.86**
Illulissat	+0.21	+0.41	+0.66	**+1.00**	**+0.43**	**+0.57**
Aasiaat	**+0.55**	**+0.56**	**+0.63**	**+1.20**	**+0.58**	**+0.73**
Kangerlussuaq	+0.40	+0.54	+0.65	+1.29	**+0.53**	**+0.72**
Sisimiut	**+0.57**	**+0.71**	**+0.76**	**+1.52**	**+0.68**	**+0.89**
Nuuk	**+0.43**	**+0.62**	+0.54	+0.65	**+0.53**	**+0.56**
Paamiut	**+0.54**	**+0.71**	+0.53	**+0.82**	**+0.59**	**+0.65**
Narsarsuaq	+0.26	**+0.62**	+0.41	+0.66	+0.43	+0.49
Qaqortoq	**+0.45**	**+0.69**	+0.49	+0.69	**+0.54**	**+0.58**
Danmarkshavn	**+0.62**	**+0.81**	+0.73	**+1.04**	**+0.72**	**+0.80**
EG1	**+0.88**	+0.43	+0.39	+0.86	**+0.56**	**+0.64**
EG2	**+1.03**	+0.44	+0.35	+0.87	**+0.61**	**+0.68**
Ittoqqortoormiit	**+0.61**	**+0.70**	**+0.80**	**+1.29**	**+0.70**	**+0.85**
EG3	**+0.95**	+0.38	+0.96	**+1.85**	**+0.77**	**+1.03**
EG4	**+0.74**	+0.26	**+0.60**	**+1.15**	**+0.53**	**+0.69**
EG5	**+0.66**	+0.26	+0.53	**+0.88**	**+0.48**	**+0.58**
Tasiilaq	**+0.74**	**+0.41**	**+0.61**	**+1.00**	**+0.59**	**+0.69**
EG6	**+0.66**	+0.51	+0.39	+0.55	**+0.52**	**+0.53**
EG7	**+0.60**	**+0.61**	+0.64	+0.63	**+0.62**	**+0.62**

717

718 **Table 3**. Linear trends of monthly and seasonal SAT data (°C decade^{-1}), 1979-2014. Bold

719 values are statistically significant at $p \leq 0.05$.

720

721

Variables	*Sept*	*Oct*	*Nov*	*Dec*	*SON*	*SOND*
WG SATs, SSTs, and Sea Ice						
Baffin Bay Sea Ice vs Baffin Bay SST	**+0.64**	**+0.77**	**+0.62**	**+0.49**	**+0.76**	**+0.76**
Baffin Bay Sea Ice Labrador Sea SST	+0.13	+0.32	**+0.42**	**+0.41**	+0.32	**+0.35**
Baffin Sea Ice vs Irminger Sea SST	+0.05	**+0.40**	**+0.49**	**+0.34**	**+0.37**	**+0.38**
Upernavik SAT vs Baffin Bay SST	**+0.51**	**+0.66**	**+0.41**	**+0.61**	**+0.67**	**+0.70**
Sisimuit SAT vs Baffin Bay SST	**+0.44**	**+0.55**	**+0.42**	**+0.69**	**+0.64**	**+0.68**
Paamiut SAT vs Labrador SST	**+0.68**	**+0.50**	**+0.37**	**+0.65**	**+0.58**	**+0.68**
Qaqortoq SAT vs Labrador SST	**+0.62**	**+0.46**	**+0.42**	**+0.64**	**+0.58**	**+0.65**
EG SATs, SSTs, and Sea Ice						
Greenland Sea Ice vs Greenland Sea SST	**+0.40**	**+0.34**	+0.15	+0.20	**+0.36**	**+0.35**
Greenland Sea Ice vs Iceland Sea SST	+0.23	**+0.51**	**+0.42**	**+0.37**	**+0.43**	**+0.46**
Greenland Sea Ice vs Irminger Sea SST	+0.12	+0.13	+0.07	+0.03	+0.12	+0.10
Danmarkshavn SAT vs Greenland Sea SST	**+0.50**	+0.14	+0.12	**+0.39**	+0.23	**+0.45**
EG1 SAT vs Greenland SST	+0.17	-0.11	+0.06	+0.20	-0.07	+0.15
Ittoqqortoormiit SAT vs Iceland Sea	**+0.42**	**+0.47**	+0.26	+0.27	**+0.40**	**+0.37**
EG4 SAT vs Iceland Sea	+0.33	+0.31	+0.12	+0.23	+0.28	**+0.35**
EG6 SAT vs Irminger Sea	**+0.34**	**+0.44**	+0.13	**+0.53**	**+0.37**	**+0.53**
EG7 SAT vs Irminger Sea	**+0.47**	**+0.46**	+0.23	**+0.54**	**+0.35**	**+0.49**

722

723 **Table 4.** A sample of detrended correlations between SATs, SSTs, and sea ice freeze onset
724 along the eastern (EG) and western (WG) Greenland. Bold values are statistically
725 significant at $p \leq 0.05$.

726

727

CP/*Mo*	*Sep*	*Oct*	*Nov*	*Dec*	*SON*	*SOND*
1	+0.11	-0.12	-0.13	**0.38**	+0.02	<-0.01
2	-0.07	+0.12	**+0.51**	-0.05	-0.01	+0.01
3	**+0.48**	**+0.56**	+0.20	**+0.36**	**+0.44**	**+0.44**
4	-0.07	+0.12	-0.20	-0.19	-0.02	-0.06
5	-0.16	**-0.65**	-0.18	-0.04	-0.15	-0.13
6	-0.16	-0.33	-0.23	-0.04	**-0.37**	-0.23
7	+0.03	-0.02	-0.19	-0.28	+0.07	-0.07
8	+0.13	-0.01	+0.17	+0.02	-0.02	+0.07
9	**-0.48**	-0.01	**-0.51**	**-0.47**	**-0.39**	**-0.47**
10	+0.28	+0.19	**+0.58**	**+0.40**	**+0.33**	**+0.34**

728

729 **Table 5**. Detrended correlations between the monthly/seasonal circulation pattern (CP)

730 frequencies and the GBI, 1979-2014. Bold values are statistically significant at $p \leq 0.05$.

731

CP/*Mo*	*Sep*	*Oct*	*Nov*	*Dec*	*SON*	*SOND*
1	**-1.20**	**-1.80**	-0.40	**3.00**	**-1.13**	-0.10
2	-0.20	-0.40	-0.60	-0.20	-0.40	-0.35
3	**2.00**	**5.60**	-0.60	0.20	**2.33**	**1.80**
4	**1.60**	**1.60**	**-2.40**	**-2.20**	0.27	-0.35
5	**-1.00**	**-2.60**	**3.20**	**1.60**	-0.13	0.30
6	-0.20	**-2.00**	**1.60**	**1.80**	-0.20	0.30
7	**1.00**	**1.00**	0.40	**1.00**	0.80	0.85
8	-0.40	**-1.20**	**-1.60**	**1.20**	**-1.07**	-0.50
9	**-1.40**	0.40	-0.60	**-5.00**	-0.53	**-1.65**
10	-0.20	-0.60	**1.00**	**-1.40**	0.07	-0.30

Table 6. Composite monthly and seasonal CP frequency anomalies for late – early Baffin Bay freeze onset years. CP occurrence differences in excess of ±1 day are bolded.

738 **Figures**

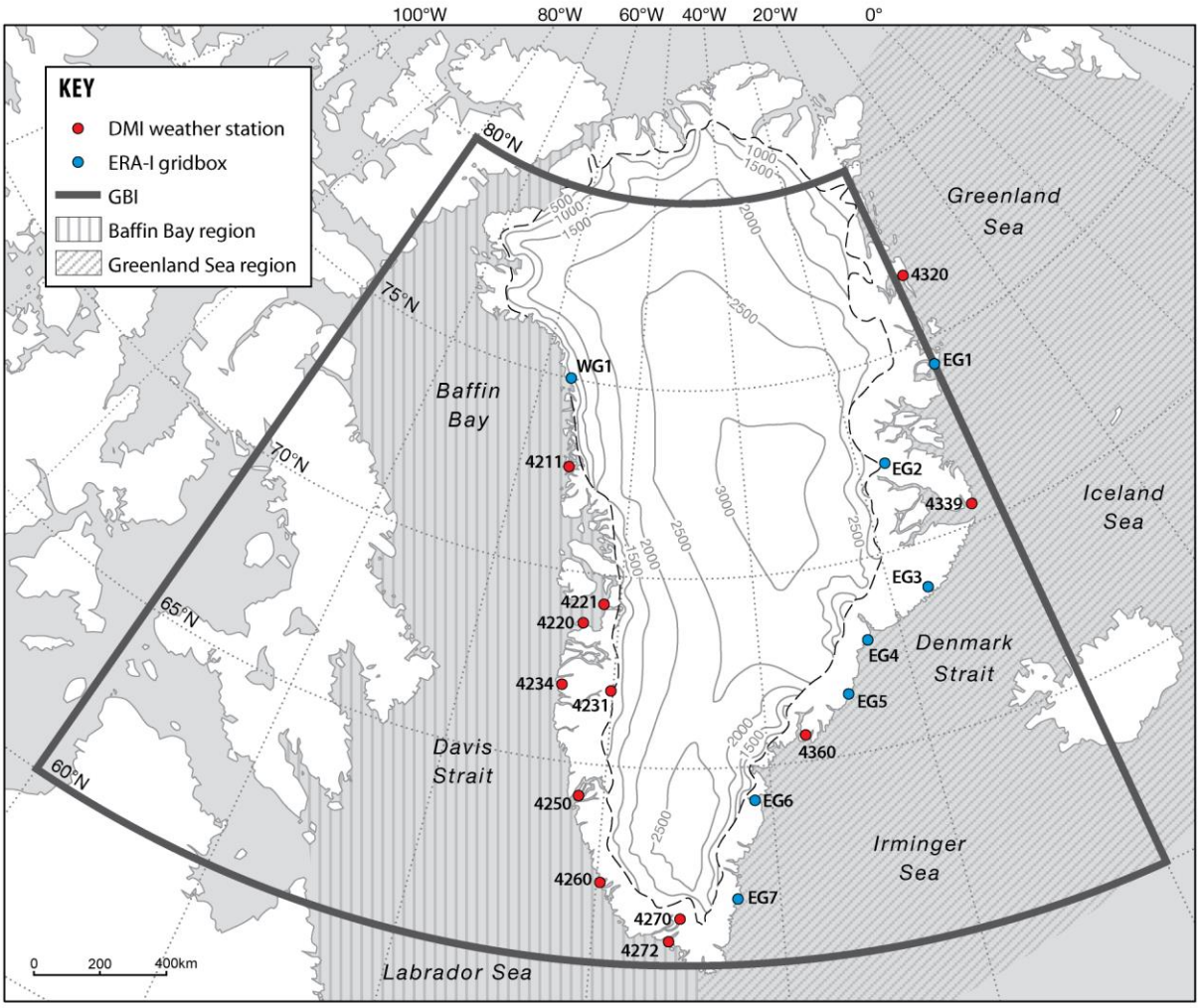

739

740 **Figure 1**. Map displaying the Greenland study area with sea ice domains, DMI and ERA-
741 Interim (i.e., ERA-I) SAT locations, and GBI domain labeled accordingly. Details involving
742 the SAT data are provided in Table 1.

743

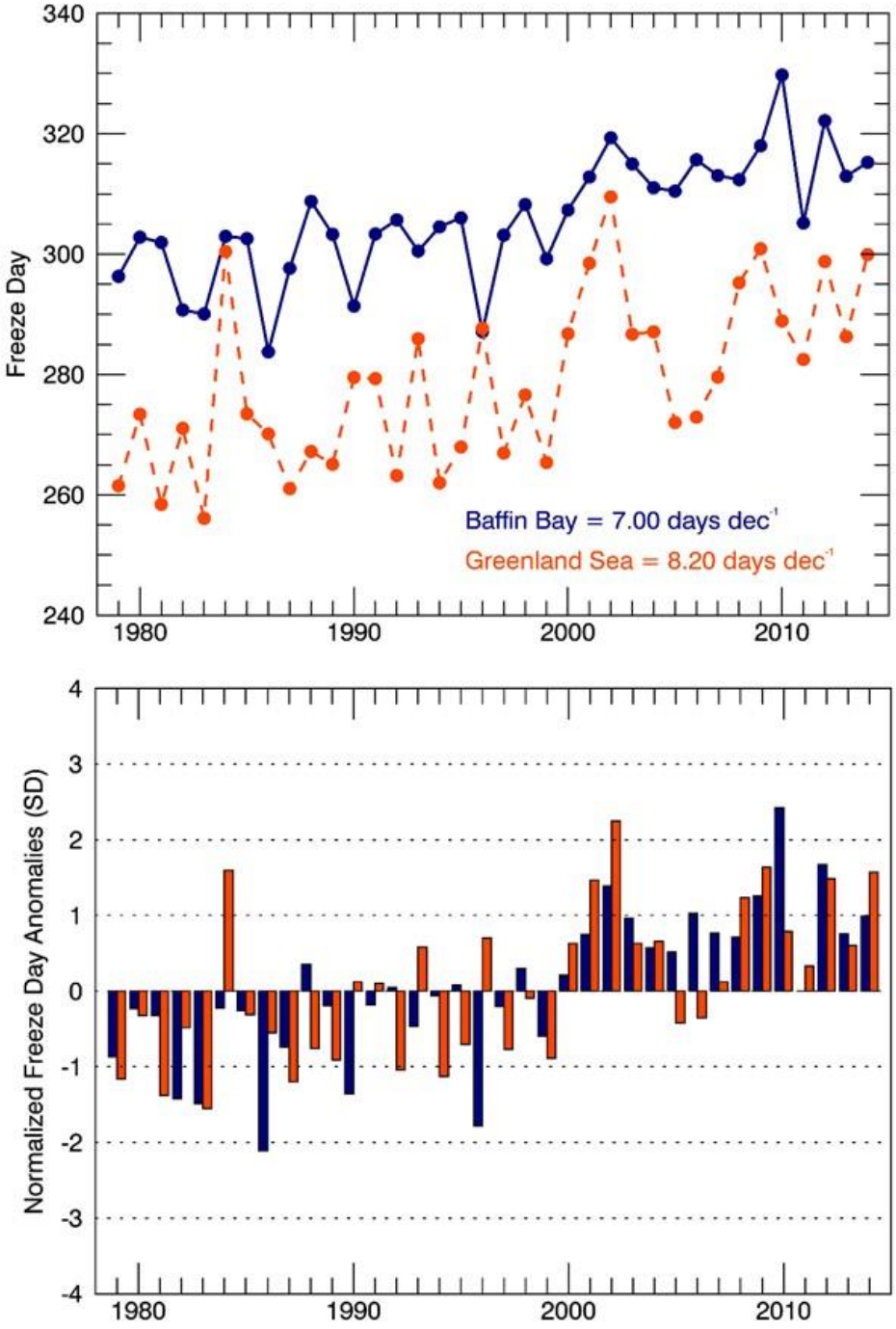

744

745 **Figure 2**. Time series of Baffin Bay and Greenland Sea freeze days with corresponding
746 linear trends (top; both significant at $p < 0.05$), and normalized freeze day anomalies
747 (bottom), 1979-2014. Anomaly units represent standard deviations (SD).

748

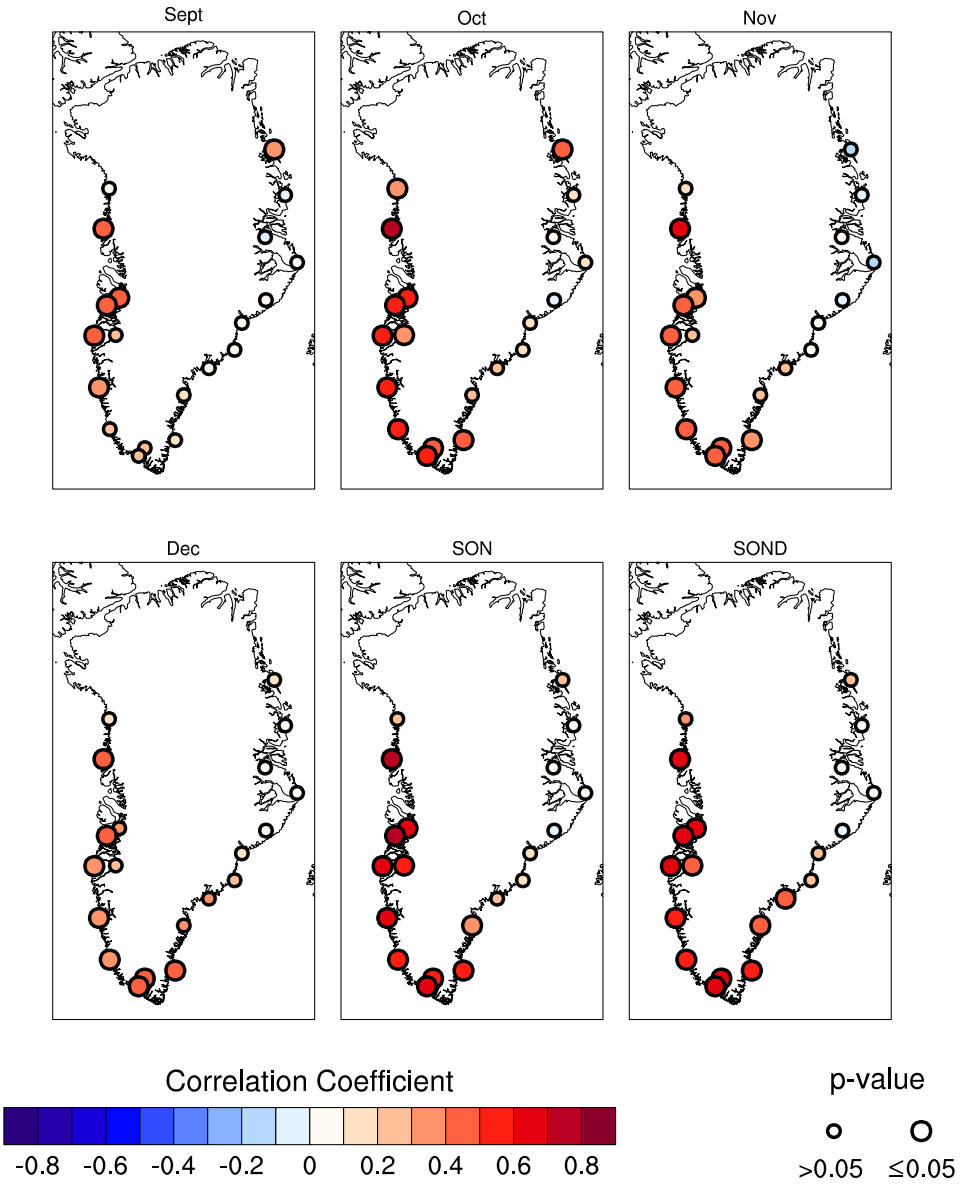

749

750 **Figure 3**. Detrended correlations between Baffin Bay freeze onset dates and the monthly

751 (Sept – Dec), autumn (SON), extended autumn (SOND) coastal SATs.

752

753

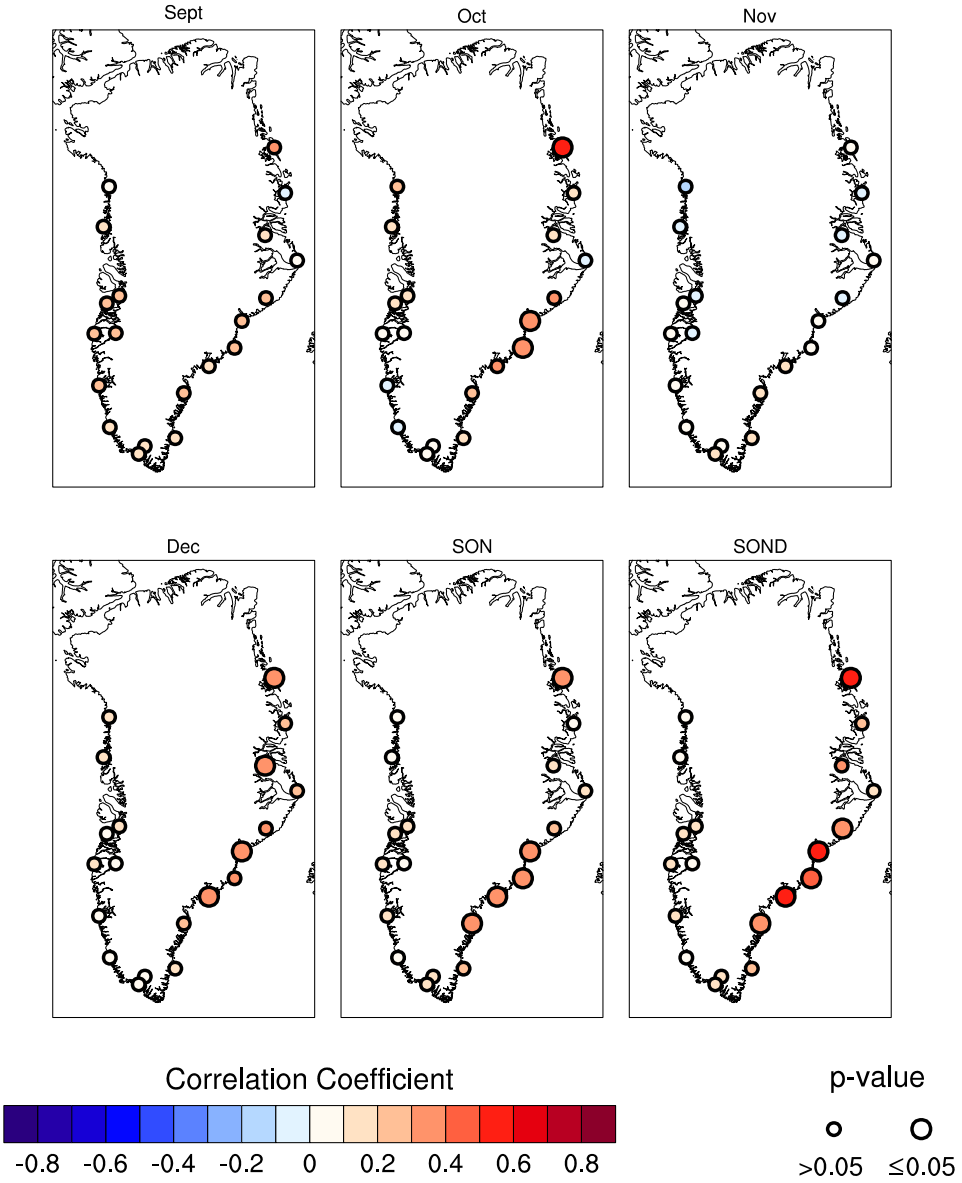

754

755 **Figure 4**. Detrended correlations between Greenland Sea freeze onset dates and the

756 monthly (Sept – Dec), autumn (SON), extended autumn (SOND) coastal SATs.

757

758

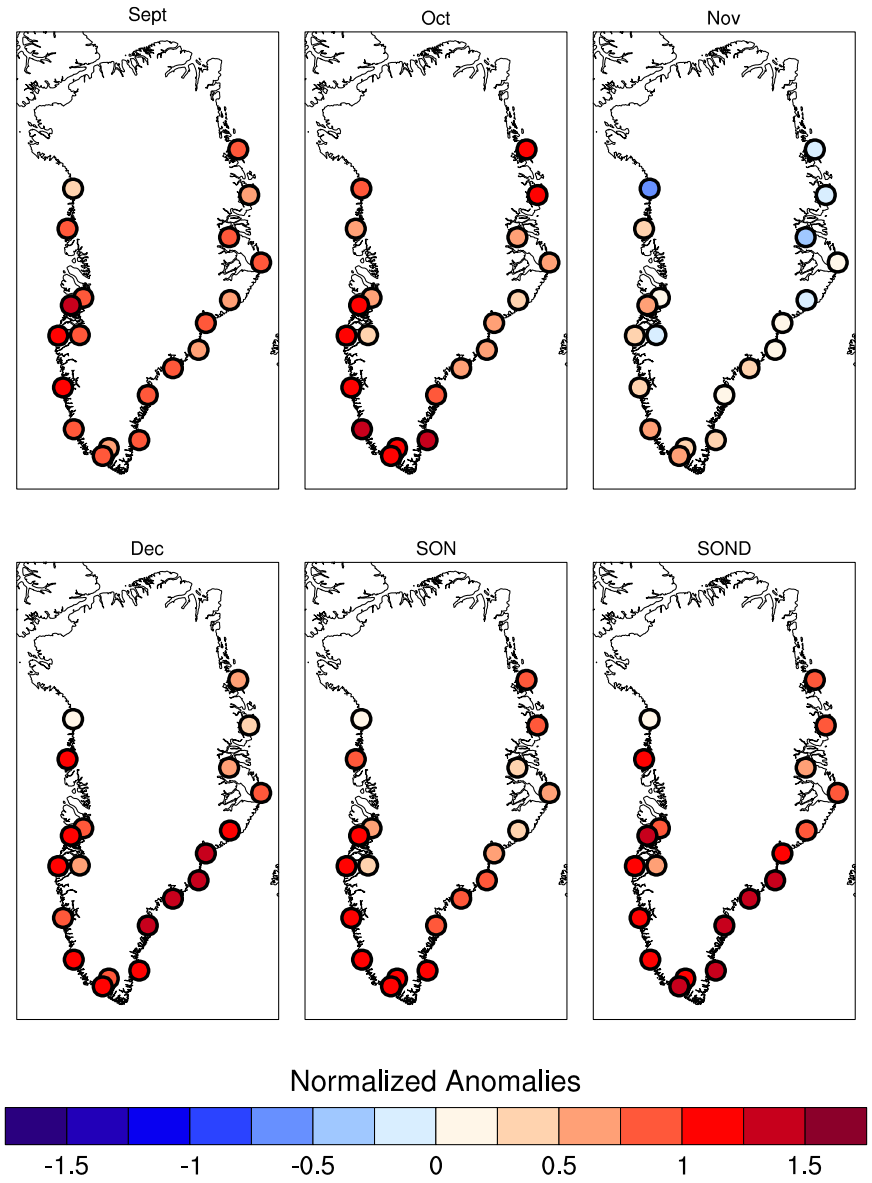

759

760 **Figure 5**. Composites of normalized SAT anomalies (in standard deviations) by

761 anomalously late Baffin Bay freeze onset years.

762

763

764

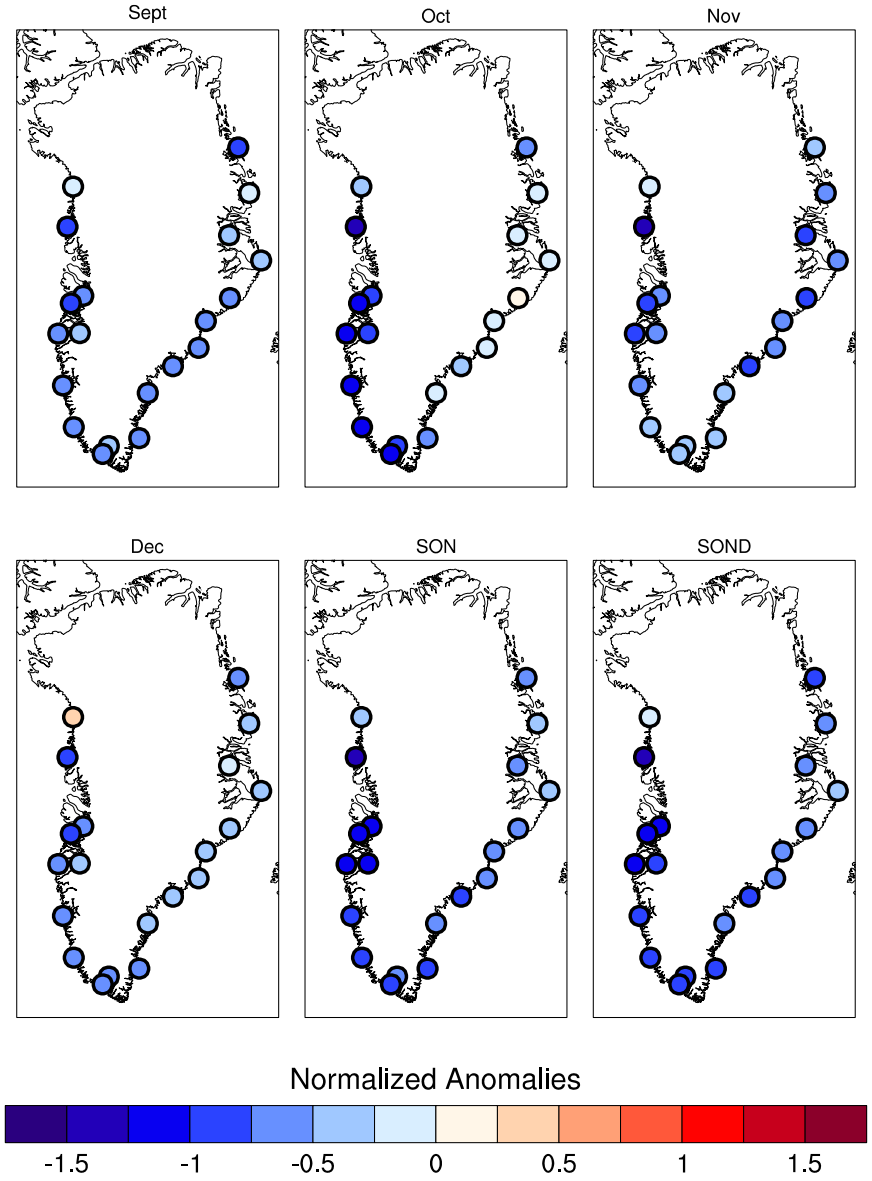

765

766 **Figure 6**. Composites of normalized SAT anomalies (in standard deviations) by

767 anomalously early Baffin Bay freeze onset years.

768

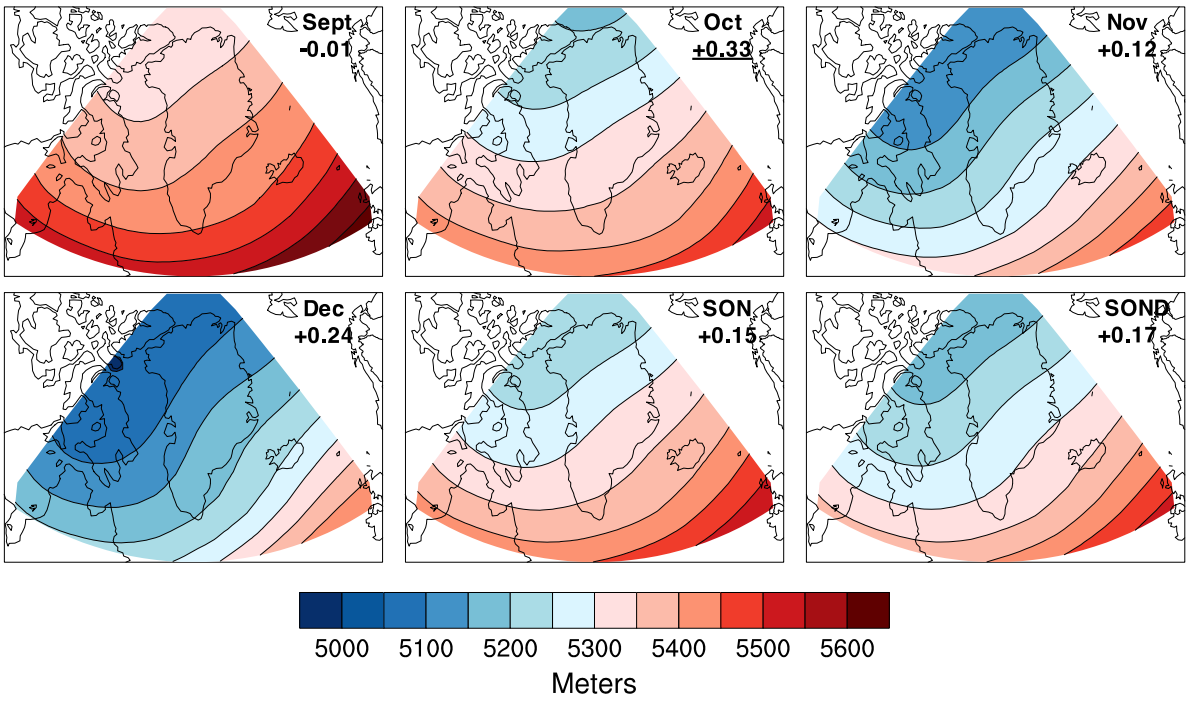

769

770 **Figure 7**. Monthly mean 500 hPa GPH patterns and corresponding GBI trends (in

771 normalized GBI values decade^{-1}), 1979-2014. Statistically significant trends at $p \leq 0.05$ are

772 underlined.

773

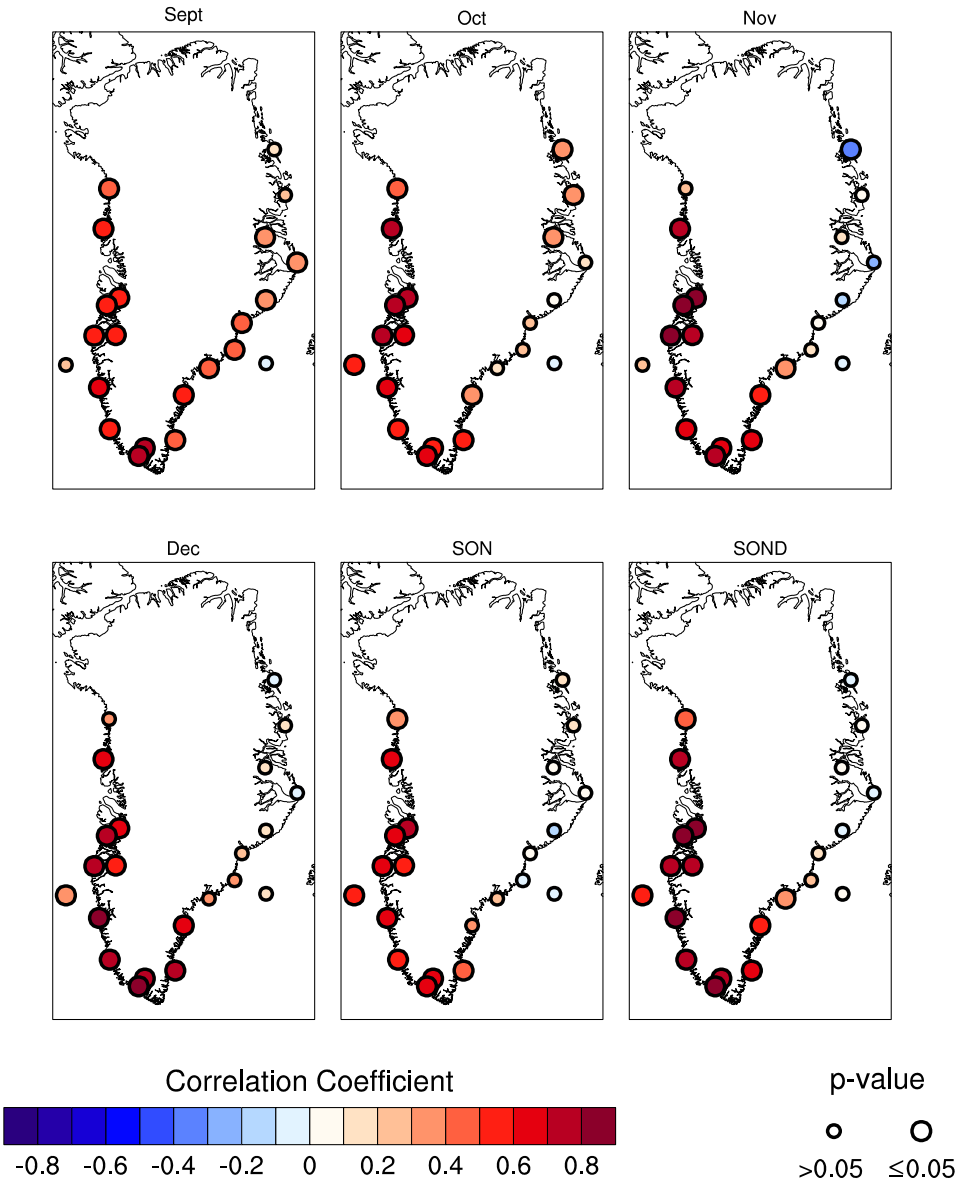

774

775 **Figure 8**. Detrended correlations between the monthly and seasonal GBI and the coastal
776 SATs and Baffin Bay and Greenland Sea freeze onset dates (signified by filled dots within
777 the respective marginal sea domains).

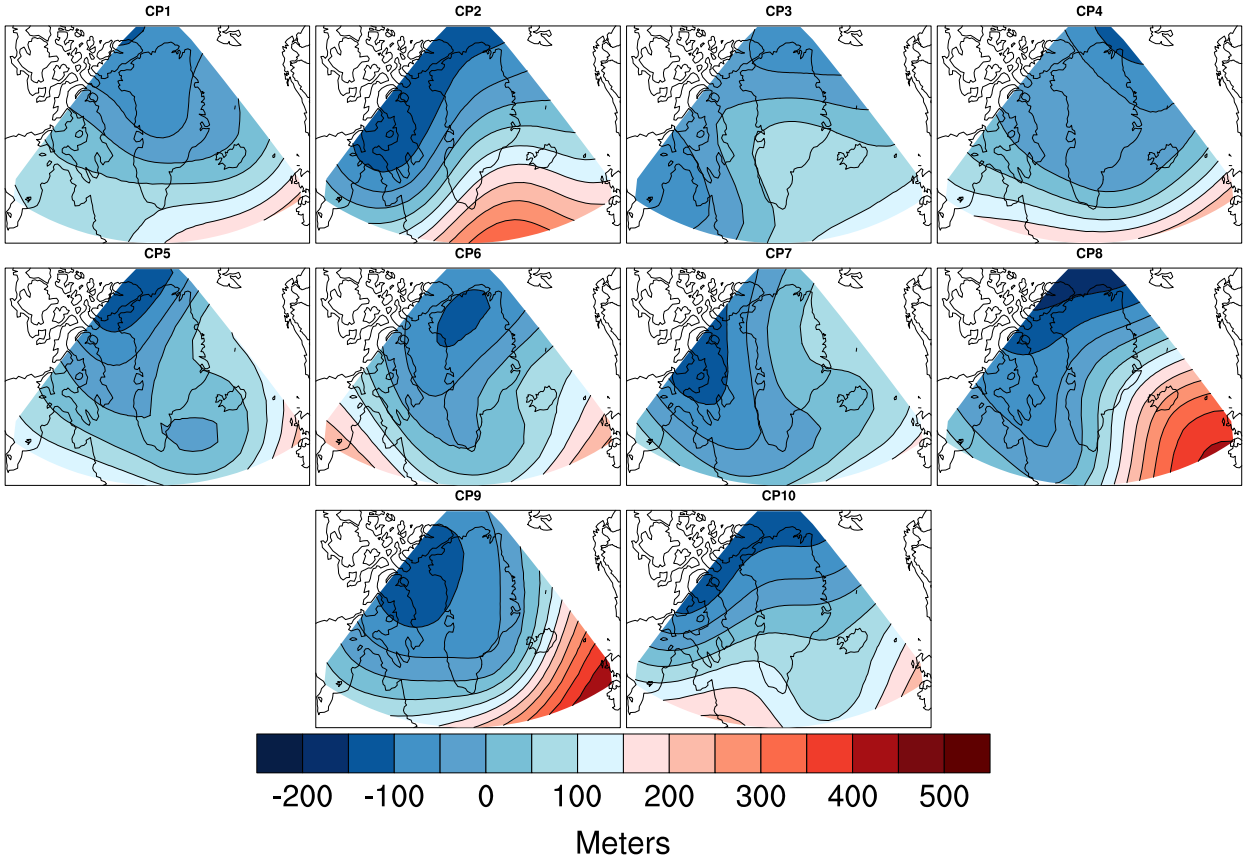

778
779 **Figure 9**. Circulation patterns (CPs) resolved from a synoptic climatology of daily 500 hPa

780 GPH spatial anomalies across Greenland for all autumn days (i.e., Sept – Dec), 1979-2014.

781

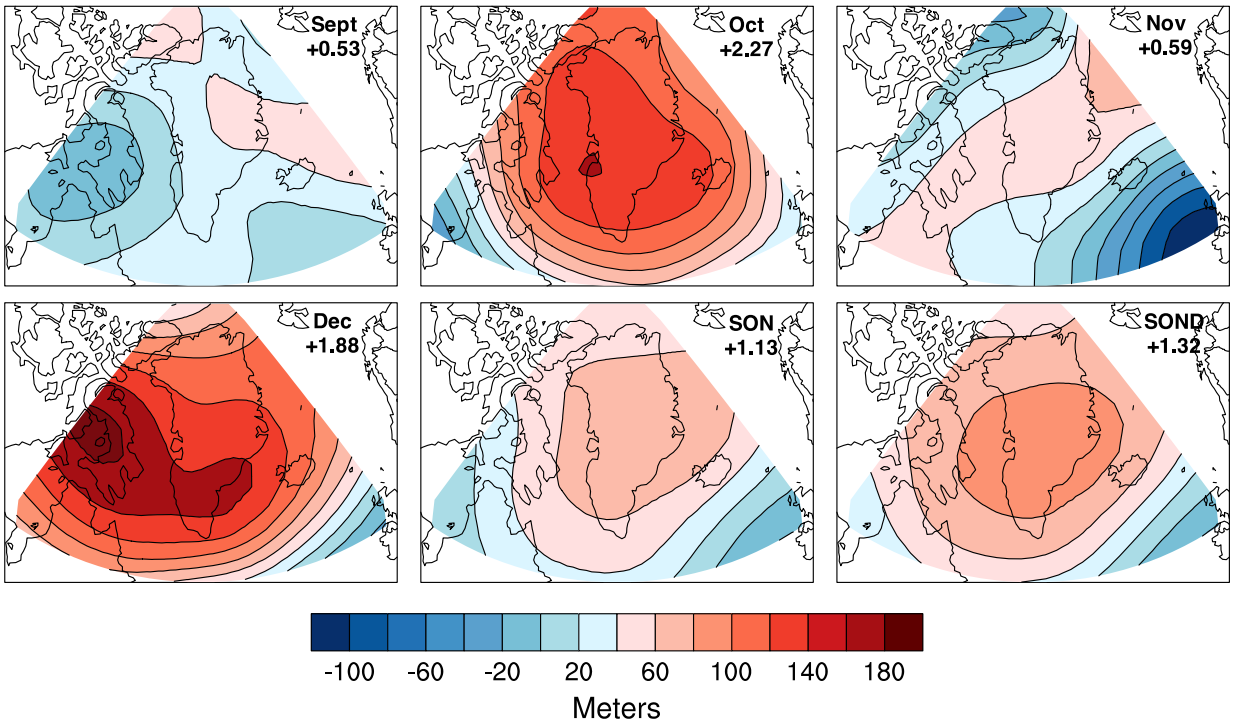

782

783 **Figure 10**. Composite net differences in 500 hPa GPH and GBI values by Baffin Bay late –

784 early freeze years, 1979-2014.

785

Supplementary Tables

CP/*Mo*	Sep	Oct	Nov	Dec	SON	SOND
1	3.97	3.56	2.69	2.08	10.22	12.31
2	2.64	2.69	3.78	3.06	9.11	12.17
3	2.33	3.19	1.86	4.39	7.39	11.78
4	3.69	3.11	2.92	3.08	9.72	12.81
5	3.86	4.28	3.33	2.56	11.47	14.03
6	3.64	3.64	2.94	2.00	10.22	12.22
7	2.44	2.17	2.92	3.25	7.53	10.78
8	2.42	2.69	3.44	3.97	8.56	12.53
9	2.61	1.81	3.00	3.86	7.42	11.28
10	2.39	3.86	3.11	2.75	9.36	12.11

Table S1. Mean frequency (in days) of CPs per month and season from 1979-2014.

CP/*Mo*	*Sep*	*Oct*	*Nov*	*Dec*	*SON*	*SOND*
1	-0.08	+0.15	+0.12	**-0.37**	<-0.01	+0.07
2	+0.12	-0.10	**-0.40**	+0.06	+0.09	-0.09
3	**-0.37**	**-0.53**	-0.27	-0.28	**-0.50**	**-0.41**
4	+0.13	-0.23	**+0.34**	+0.21	+0.04	+0.13
5	+0.16	**+0.53**	+0.03	+0.07	+0.11	+0.10
6	+0.20	**+0.40**	+0.16	+0.07	**+0.33**	+0.12
7	-0.22	+0.05	+0.21	+0.23	-0.11	<+0.01
8	-0.03	+0.05	-0.08	-0.06	+0.01	-0.04
9	+0.20	+0.02	**+0.38**	**+0.38**	**+0.34**	**+0.48**
10	-0.15	-0.18	**-0.53**	**-0.41**	-0.20	-0.27

Table S2. Detrended correlations between the monthly and seasonal CP frequencies and the NAO, 1979-2014. Bold values are statistically significant at $p \leq 0.05$.

CP/*Mo*	*Sep*	*Oct*	*Nov*	*Dec*	*SON*	*SOND*
1	+0.01	+0.16	+0.08	-0.32	+0.01	+0.08
2	+0.05	-0.01	-0.26	-0.02	+0.09	-0.05
3	-0.22	**-0.50**	**-0.48**	**-0.41**	**-0.47**	**-0.45**
4	+0.27	-0.28	**+0.38**	+0.28	-0.05	+0.07
5	+0.14	**+0.47**	+0.01	+0.06	+0.10	+0.11
6	+0.05	+0.31	+0.09	+0.10	+0.11	-0.02
7	**-0.42**	-0.22	-0.11	+0.12	**-0.40**	-0.19
8	+0.19	+0.21	+0.14	+0.15	+0.24	+0.16
9	-0.08	+0.03	+0.32	**+0.35**	**+0.36**	**+0.49**
10	-0.02	-0.08	-0.30	**-0.33**	+0.07	-0.16

Table S3. Detrended correlations between the monthly and seasonal CP frequencies and the AO, 1979-2014. Bold values are statistically significant at $p \leq 0.05$.

CP/*Mo*	*Sep*	*Oct*	*Nov*	*Dec*	*SON*	*SOND*
1	**-2.26**	-0.60	**-1.07**	0.19	**-1.31**	-0.93
2	0.67	-0.14	-0.45	**2.00**	0.02	0.52
3	**-1.07**	**-2.07**	**1.76**	0.10	-0.46	-0.32
4	0.05	-0.36	**-1.71**	**-2.38**	-0.67	**-1.10**
5	**-3.38**	**1.81**	**1.86**	**-1.71**	0.10	-0.36
6	**1.33**	0.12	-0.21	-0.86	0.41	0.10
7	0.60	**2.33**	0.07	**1.95**	**1.00**	**1.24**
8	**2.10**	-0.48	**-1.57**	**1.52**	0.02	0.39
9	**3.31**	-0.38	-0.07	0.79	0.95	0.91
10	**-1.33**	-0.24	**1.40**	**-1.60**	-0.06	-0.44

Table S4. Composite monthly and seasonal frequency anomalies for late – early Greenland Sea freeze onset years. CP occurrence differences in excess of ±1 day are bolded.

807 **Supplementary Figures**

808

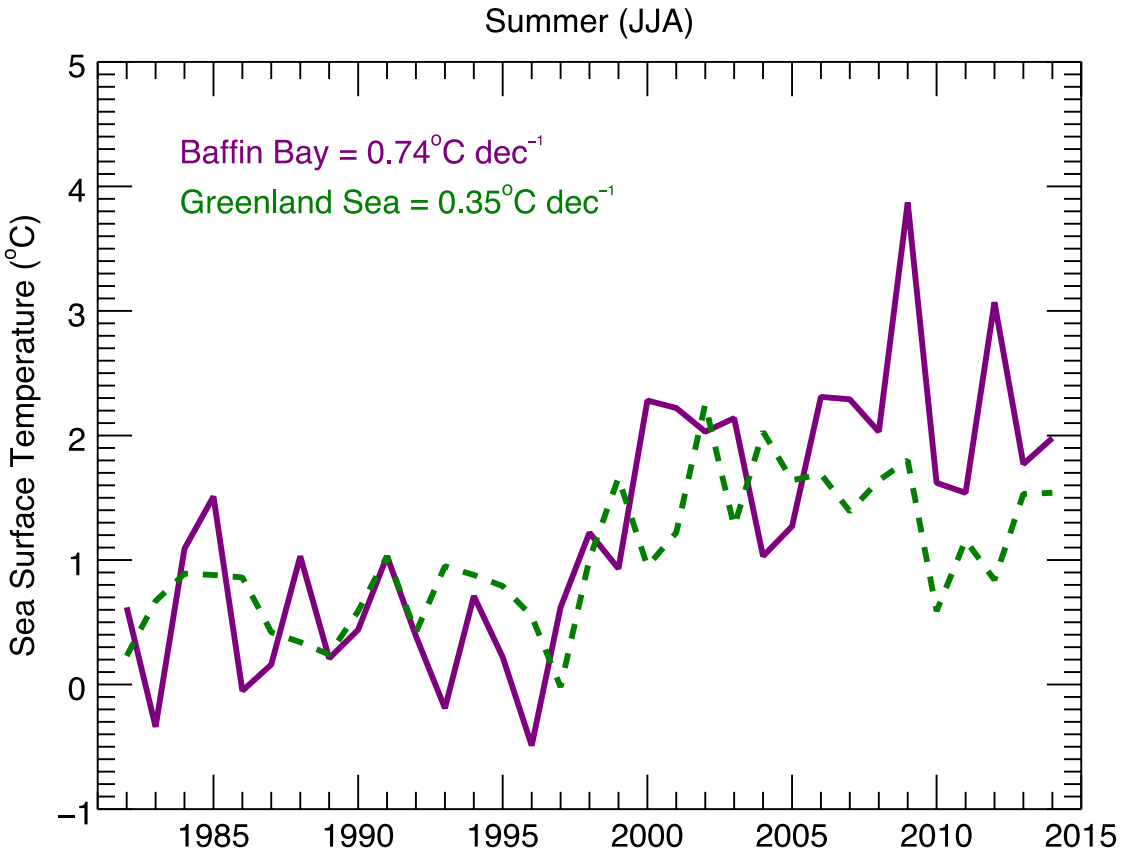

809

810 **Figure S1.** Summer (JJA) sea surface temperature (SST) time series for Baffin Bay and

811 Greenland Sea. Linear trends are shown in °C decade^{-1} and both seasonal SST time series

812 are significant at $p \leq 0.05$.

813

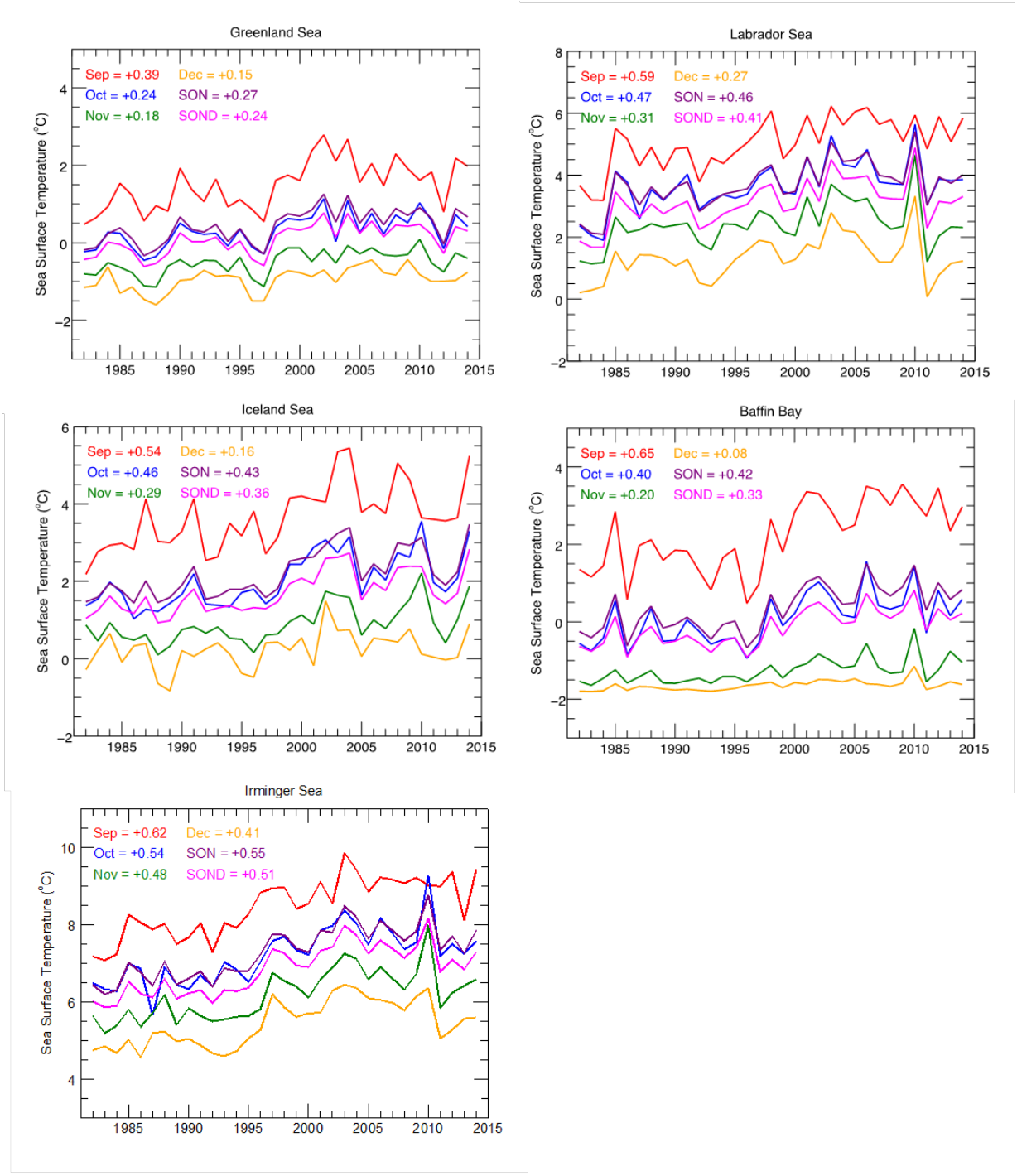

814

815 **Figure S2.** Autumn sea surface temperature (SST) time series for the marginal seas of the

816 Greenland Sea (left column) and Baffin Bay (right column) sea ice domains, 1982-2014.

817 Linear trends are shown in °C decade^{-1} and all monthly and seasonal SST time series are

818 significant at $p \leq 0.05$.

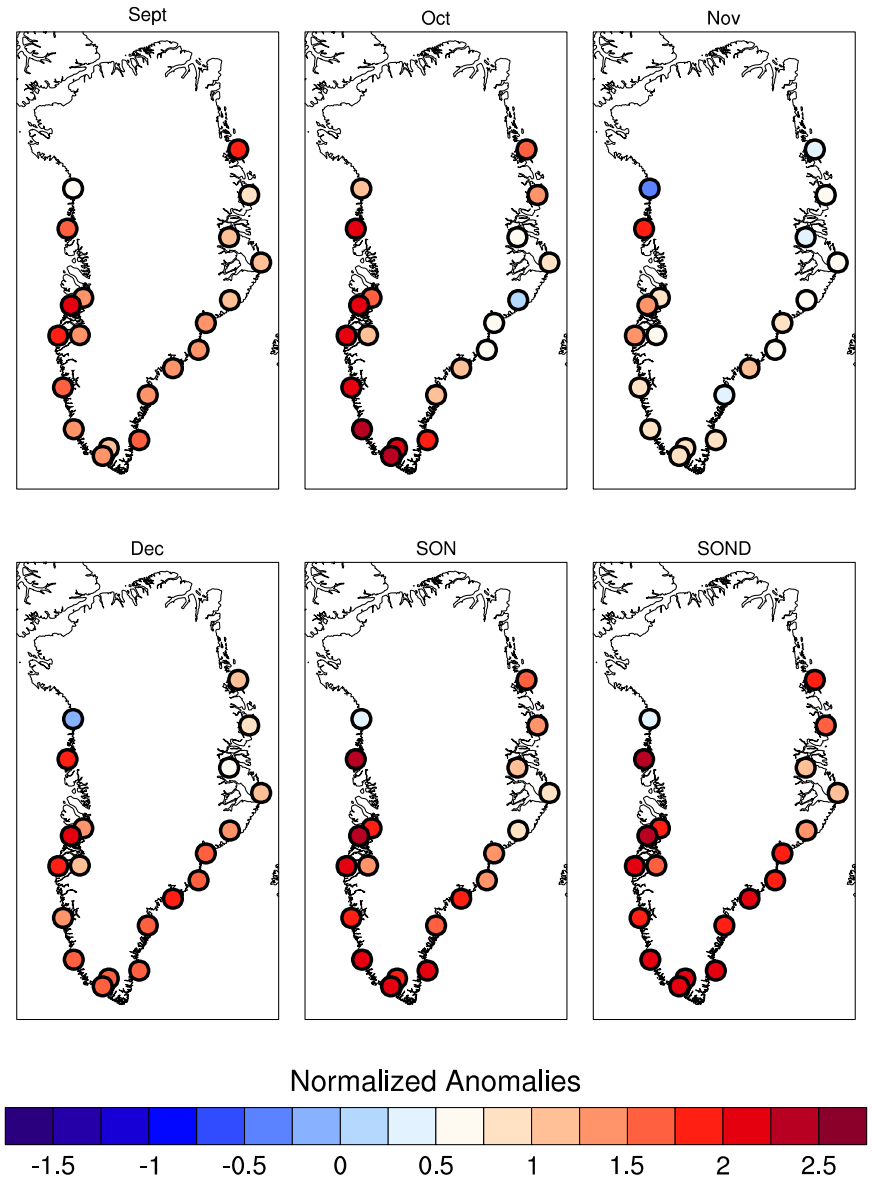

819

820 **Figure S3**. Difference in normalized SAT anomalies (in standard deviations) by Baffin Bay

821 late – early freeze onset anomalies.

822

823

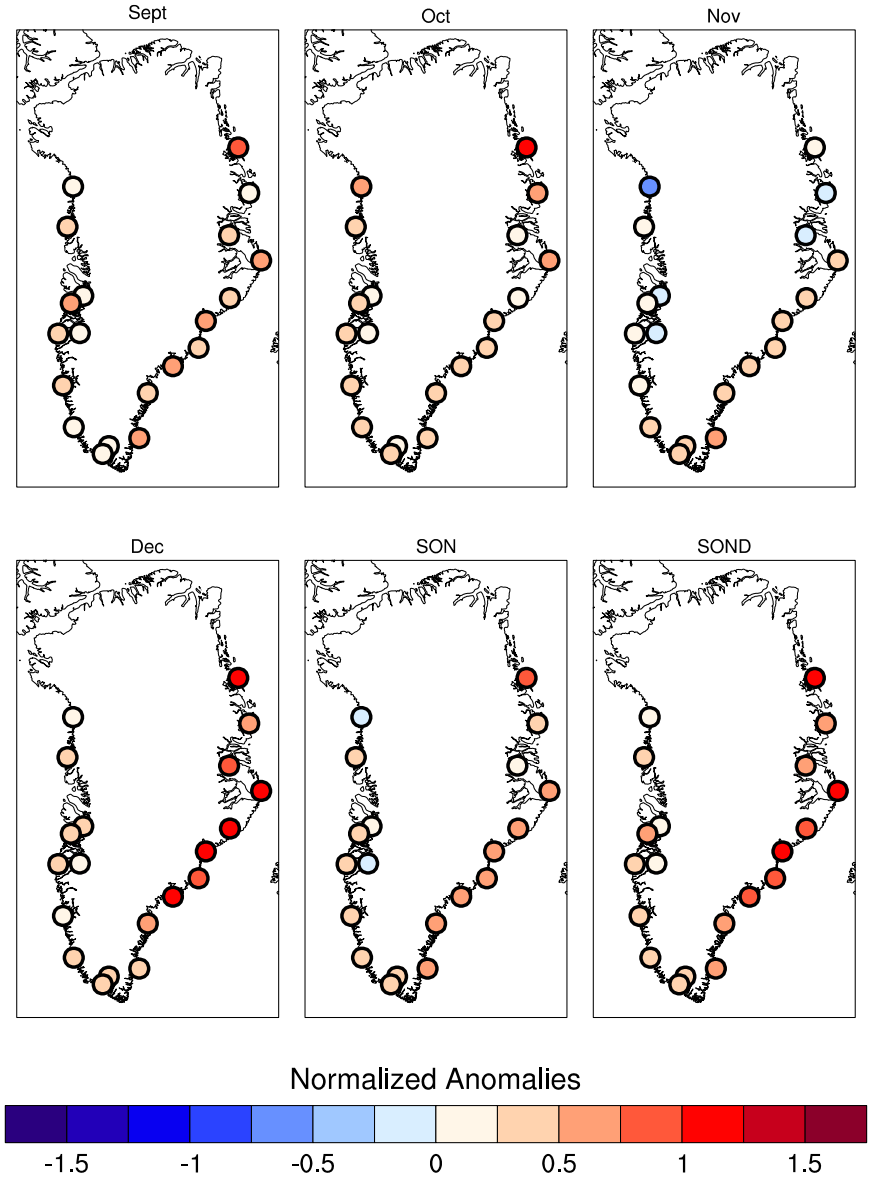

824

825 **Figure S4**. Composites of normalized SAT anomalies (in standard deviations) by

826 anomalously late Greenland Sea freeze onset years.

827

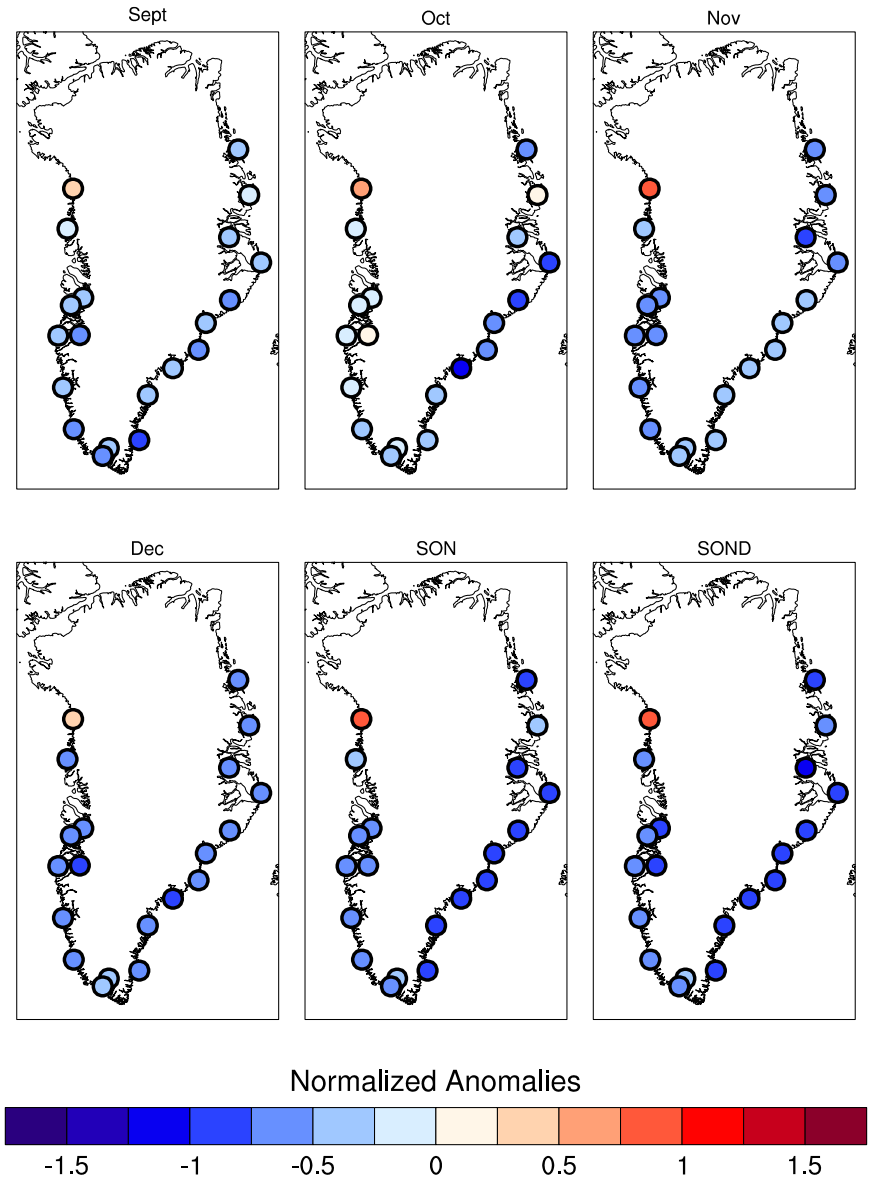

828

829 **Figure S5**. Composites of normalized SAT anomalies (in standard deviations) by

830 anomalously early Greenland Sea freeze onset years.

831

832

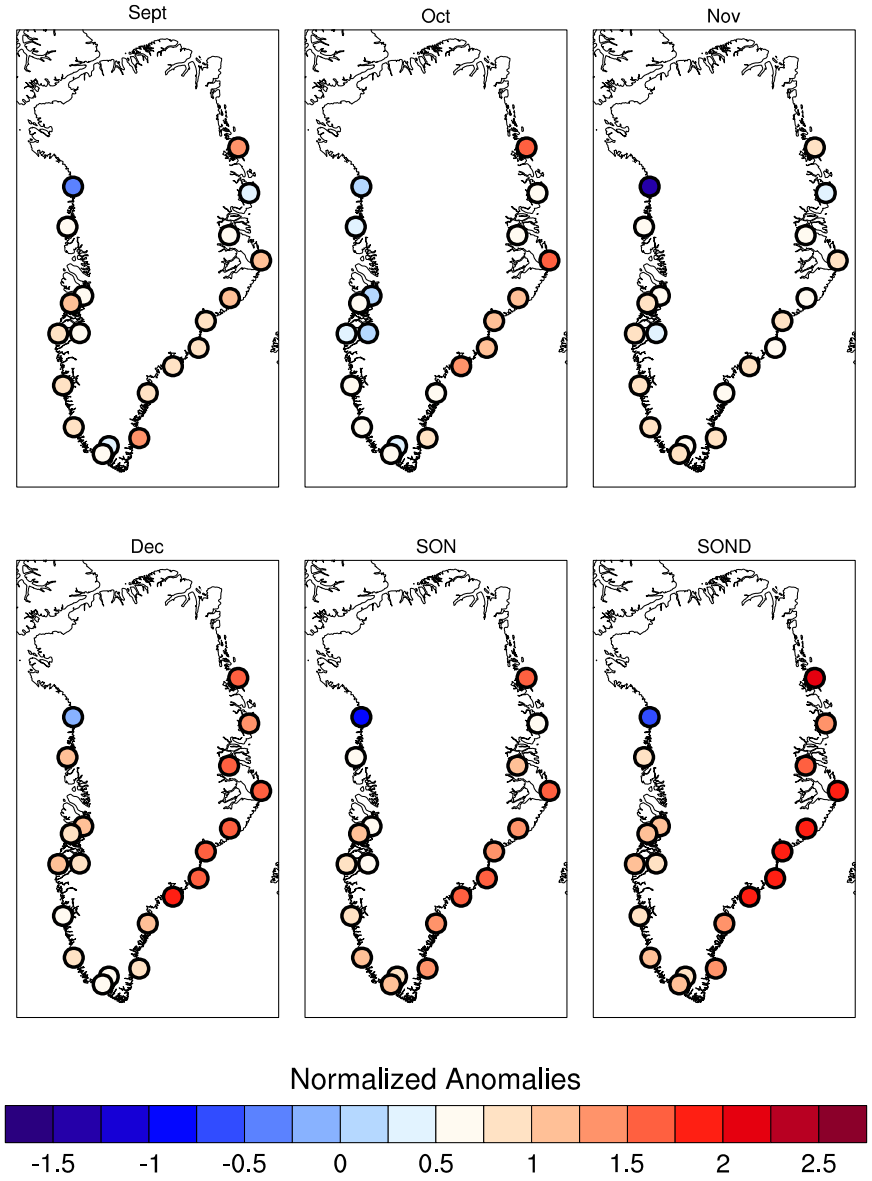

833

834 **Figure S6**. Difference in normalized SAT anomalies (in standard deviations) by Greenland

835 Sea late – early freeze onset anomalies.

836

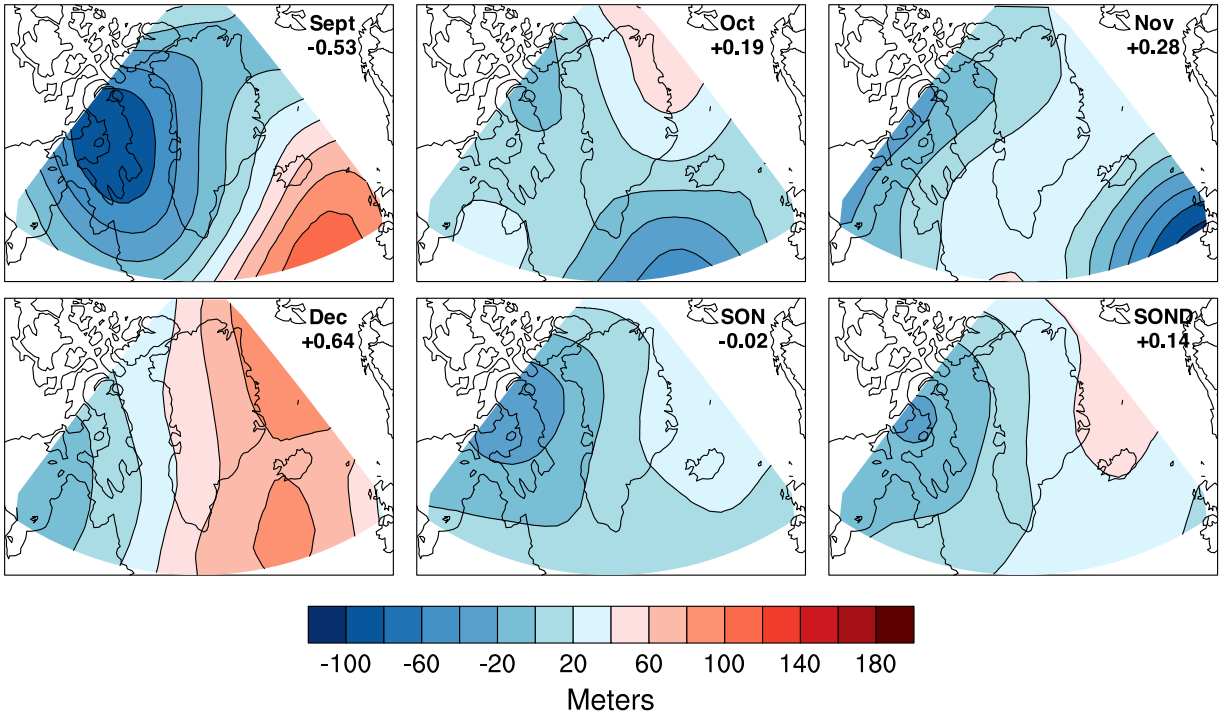

Figure S7. Composite net differences in 500 hPa GPH and GBI values by Greenland Sea late – early freeze years, 1979-2014.